The methamphetamine-induced RNA targetome of hnRNP H in *Hnrnph1* mutants showing reduced dopamine release and behavior

Qiu T. Ruan[1,2,3], Michael A. Rieger[4], William B. Lynch[2,5], Jiayi W. Cox[6], Jacob A. Beierle[1,2,3], Emily J. Yao[2], Amarpreet Kandola[2], Melanie M. Chen[2], Julia C. Kelliher[2], Richard K. Babbs[2], Peter E. A. Ash[7], Benjamin Wolozin[7], Karen K. Szumlinski[8], W. Evan Johnson[9], Joseph D. Dougherty[4], and Camron D. Bryant[1,2,3]*

1. Biomolecular Pharmacology Training Program, Department of Pharmacology and Experimental Therapeutics, Boston University School of Medicine
2. Laboratory of Addiction Genetics, Department of Pharmacology and Experimental Therapeutics and Psychiatry, Boston University School of Medicine
3. Transformative Training Program in Addiction Science, Boston University School of Medicine
4. Department of Genetics, Department of Psychiatry, Washington University School of Medicine
5. Graduate Program for Neuroscience, Boston University
6. Programs in Biomedical Sciences, Boston University School of Medicine
7. Department of Pharmacology and Experimental Therapeutics and Neurology, Boston University School of Medicine
8. Department of Psychological and Brain Sciences, University of California, Santa Barbara
9. Department of Medicine, Computational Biomedicine, Boston University School of Medicine

***Corresponding Author**

Camron D. Bryant, Ph.D.

Department of Pharmacology and Experimental Therapeutics and Department of Psychiatry

72 E. Concord St. L-606C

Boston, MA 02118 USA

E: camron@bu.edu

P: (617) 358-9581

HIGHLIGHTS

- The hnRNP H RNA targetome contains an enrichment of G-rich binding motifs within introns
- The hnRNP H RNA targetome reveals gene networks enriched for synaptic function
- *Hnrnph1* mutation and methamphetamine treatment induce changes in RNA-binding targets of hnRNP H
- Targetome, transcriptome, and spliceome analysis triangulated on *Cacna2d2* as a methamphetamine-induced regulatory target with potential physiological relevance to synaptic transmission and behavior

SUMMARY

We previously identified *Hnrnph1* (heterogeneous nuclear ribonucleoprotein H1) as a quantitative trait gene underlying reduced methamphetamine behavioral sensitivity. Mice with a heterozygous frameshift deletion in the first coding exon of *Hnrnph1* showed reduced methamphetamine-induced dopamine release and behaviors. To inform the mechanism linking hnRNP H dysfunction with reduced methamphetamine-induced dopamine release and behavior, we surveyed the RNA targetome of hnRNP H via cross-linking immunoprecipitation coupled with RNA-sequencing in striatal tissue at baseline and at 30 min post-methamphetamine (2 mg/kg, i.p.). Methamphetamine induced opposite changes in RNA-binding targets of hnRNP H in *Hnrnph1* mutants versus wild-types, including 3'UTR targets in mRNAs enriched for synaptic proteins involved in dopamine release and excitatory synaptic plasticity. Targetome, transcriptome, and spliceome analyses triangulated on a methamphetamine-induced upregulation of *Cacna2d2* transcript and decreased 3'UTR usage in hyposensitive *Hnrnph1* mutants. Our study identifies a dynamic methamphetamine-induced RNA targetome of hnRNP H that has the potential to rapidly regulate gene expression, synaptic transmission, plasticity, and behavior.

KEY WORDS: GWAS, amphetamine, cocaine, substance use disorder (SUD), psychostimulant use disorder (PUD), psychiatric genetics, PGC-SUD, RNA-binding protein

INTRODUCTION

Methamphetamine is a highly addictive psychostimulant with a strong potential for misuse along with neurotoxic effects on the central nervous system (Galbraith, 2015; Kish, 2008). In the United States, the drug overdose death rate involving psychostimulants increased nearly 5-fold from 2012 through 2018 and continues to rise (Hedegaard et al., 2020). There are currently no FDA-approved treatments for methamphetamine dependence. Understanding the cell biological mechanisms and adaptations underlying methamphetamine's psychostimulant properties has the potential to inform new therapeutic avenues.

Methamphetamine-induced dopamine release in the striatum is mediated through displacement of dopamine from synaptic vesicles through the vesicular monoamine transporter and the reverse transport of dopamine into the synapse through the dopamine transporter (Fleckenstein and Hanson, 2003; Siciliano et al., 2014). Methamphetamine-induced dopamine release contributes to the addiction liability of methamphetamine (Baumann et al., 2002). However, the rapid cell biological adaptations following acute methamphetamine administration are not fully understood.

Genetic factors contribute to risk for developing substance use disorders, including addiction to psychostimulants such as methamphetamine (Ducci and Goldman, 2012; Goldman et al., 2005). The application of rodent forward genetic studies to psychostimulant addiction-relevant traits has led to the discovery of several genes associated with behavior, including *Fam53b* (Dickson et al., 2015), *Taar1* (Reed et al., 2018; Shi et al., 2016), *Grm2* (Zhou et al., 2013), and *Csnk1e* (Bryant et al., 2012). Notably, *FAM53B* was also identified in human GWAS of cocaine addiction (Gelernter et al., 2014), highlighting the translational relevance of rodent models.

RNA binding proteins (**RBPs**) such as hnRNP H1 (coded by *Hnrnph1*) regulate each step of the RNA life cycle from processing to localization to degradation (Darnell, 2013; Hentze et al., 2018). Mutations in genes encoding RBPs including *FMR1* (Verkerk et al., 1991), *PTBP1* (Qian et al., 2020), *EFTUD2* (Lines et al., 2012), and *SF3B4* (Bernier et al., 2012) are implicated in neurodevelopmental and neuropsychiatric disorders, including substance use disorders (Bryant and Yazdani, 2016). Coding mutations in *HNRNPH1* and the gene paralog *HNRNPH2* are associated with severe neurodevelopmental disorders comprising mental retardation and intellectual disability (Pilch et al., 2018; Reichert et al., 2020). Deletion of FMRP disrupts dopaminergic neuron development and alters psychostimulant-induced neuroplasticity and behavior (Fish et al., 2013; Fulks et al., 2010; Smith et al., 2014). Alternative splicing of exon 2 and transcriptional regulation of *Oprm1* (mu opioid receptor) is mediated through the binding of hnRNP H1 and recruitment of other hnRNPs to its intronic AGGG sequence (Xu et al., 2014).

We previously identified *Hnrnph1* as a quantitative trait gene for methamphetamine stimulant sensitivity in mice (Yazdani et al., 2015) and have since identified a set of quantitative trait variants within the 5'UTR associated with both decreased hnRNP H protein and methamphetamine-induced behavior (Ruan et al., 2020b).

Furthermore, mice heterozygous for a 16 bp indel within the first coding exon of *Hnrnph1* (referred to as *Hnrnph1* mutants) showed reduced sensitivity to methamphetamine-induced locomotor activity, reward, and reinforcement and reduced methamphetamine-induced dopamine release in the ventral striatum (Ruan et al., 2020a). Synaptosomal proteomic analysis of the striatum following methamphetamine administration identified opposite changes in the localization of several mitochondrial proteins in *Hnrnph1* mutants compared to wild-types, suggesting synaptic mitochondrial dysfunction as a cell biological mechanism underlying reduced methamphetamine-induced dopamine release and addiction-related behaviors (Ruan et al., 2020a).

*Hnrnph1 (*heterogeneous nuclear ribonucleoprotein H1; codes for hnRNP H1) codes for an RBP that is expressed throughout the brain and belongs to the hnRNP H/F subfamily of hnRNP RBPs that engage in several aspects of RNA processing including pre-mRNA splicing, mRNA stability, transcriptional and translational regulation, and polyadenylation control (Arhin et al., 2002; Geuens et al., 2016; Han et al., 2010; Honoré et al., 1995; Uren et al., 2016). During cellular stress, RBPs (Markmiller et al., 2018) including hnRNP H (Wall et al., 2020), hnRNP A1 (Guil et al., 2006), and hnRNP K (Fukuda et al., 2009) localize to stress granules in the cytoplasm to sequester mRNAs from being translated. The highly dynamic formation of stress granules induced by cellular stress suggests that the interaction of hnRNP H with its mRNAs can change rapidly in response to environmental stimuli, including stress-induced signaling.

Methamphetamine is a substrate for both the dopamine transporter and the vesicular monoamine transporter and causes reverse transport of dopamine from the presynaptic terminal and an increase in dopamine at the synaptic cleft (Fleckenstein et al., 2009; Siciliano et al., 2014). Methamphetamine-induced dopamine release within the nucleus accumbens contributes to its acute stimulatory, rewarding, and reinforcing properties (Wise, 2004). Because we observed reduced methamphetamine-induced dopamine release and behavior in *Hnrnph1* mutants (Ruan et al., 2020a; Yazdani et al., 2015), in the present study, we sought to identify the RNA-binding targets of hnRNP H in the striatum, a brain region important for stimulant and addictive properties of methamphetamine. We examined changes in RNA-binding, mRNA expression, and mRNA splicing in *Hnrnph1* mutants versus wild-types, both at baseline and in response to acute administration of methamphetamine. We hypothesized that *Hnrnph1* mutation would disrupt RNA-binding, splicing, and expression at baseline as well as the dynamics of these cellular processes in response to methamphetamine. hnRNP H is primarily localized to the nucleus but also has recently been detected in the cytoplasm (Wall et al., 2020). Thus, we predicted that we would identify both presynaptic (dopaminergic terminals) and post-synaptic (striatal neurons) RNA targets relevant to dopaminergic transmission that could inform the molecular mechanisms hnRNP H dysfunction in *Hnrnph1* mutants that underlie decreased methamphetamine-induced dopamine release and behavior.

RESULTS

Hnrnph1 mutants showed reduced methamphetamine-induced locomotor activity

Mice were subjected to a 3-day behavioral protocol to assess methamphetamine-induced locomotor activity prior to tissue collection on Day 3. Performing CLIP specifically in the striatum required a large quantity of tissue. For this reason, we pooled striata (left and right) from four mice (2 females and 2 males per pooled sample) for each condition (**Table S1**). The data reported here represent the average locomotor activity from four mice per replicate for each of the four conditions listed. On the saline-treated Days (Days 1 and 2), there was no difference in locomotor activity (**Figure S1**). On Day 3, following an acute dose of methamphetamine at 2 mg/kg, *Hnrnph1* mutants showed reduced locomotor activity versus wild-types (**Figure 1A**) (Ruan et al., 2020a; Yazdani et al., 2015). Importantly, there was no effect of genotype in response to saline on Day 3 (**Figure 1A**), indicating that the genotype effect was specific to methamphetamine treatment. The striata were then immediately harvested from each mouse at 30 min post-injection on Day 3 for CLIP-seq processing.

hnRNP H binding sites contain G-rich binding motifs that are enriched in the intronic regions

Accumulating evidence from our lab indicates a role of hnRNP H in methamphetamine addiction liability (Ruan et al., 2020a). Defining the set of RNA targets in brain tissue that are differentially regulated by hnRNP H in *Hnrnph1* mutants in response to methamphetamine could inform key mechanisms underlying decreased dopamine release and behavior. To identify the *in vivo* hnRNP H targets, we performed CLIP using an antibody specific for hnRNP H in the striatum of *Hnrnph1* mutants versus wild-types, following saline or methamphetamine treatment. We previously validated this antibody to be specific for the C-terminus of hnRNP H via immunoadsorption with a blocking peptide for the epitope (Ruan et al., 2018). Here, we show that the antibody specifically pulled down hnRNP H at 50 kDa with no signal detected using rabbit IgG (**Figure S2A**; Lane 6 versus Lane 3). Importantly, we used stringent lysis and wash conditions as published (Van Nostrand et al., 2016). Twenty µg of hnRNP H antibody was the optimal amount needed as indicated by visual inspection of the band intensity (**Figure S2B**).

Our CLIP procedure resulted in RNA-specific pulldown of hnRNP H-RNA complexes. RNase fragmented the CLIP samples into different sizes in a concentration-dependent manner (**Figure 1B**; from left to right, Lanes 3 – 6) indicating the hnRNP H CLIP was RNA-dependent. Longer incubation of CLIP samples with RNase resulted in lower amount of RNA, providing further support that hnRNP H CLIP was RNA-dependent (**Figure S2C**; Lanes 2-5). Negative controls included immunoprecipitation (**IP**) from uncrosslinked sample (**Figure 1B**; Lane 1) and IP using rabbit IgG from wild-type striatal tissues (**Figure 1B**; Lane 2). No RNA was detected in these two negative control samples (**Figure 1B**; Lanes 1 and 2), indicating the need for UV-crosslinking for RNA pull down and demonstrating the specificity of hnRNP H pull down. We chose a region 30 – 70 nucleotides in size (50 – 80 kDa) for RNA extraction to capture the targets of hnRNP H *in vivo* (**Figure 1B**). The cDNA libraries generated from the CLIP samples of the IgG IPs did not yield any detectable PCR bands using gel electrophoresis, even after 28 PCR cycles (**Figure S2D**). For this reason, none of the four IgG

cDNA libraries were subjected to sequencing. However, for the CLIP samples, DNA bands corresponded to the correct size of the cDNA library (> 150 bp) and were detected after 18 PCR cycles (**Figure S2E**). We subjected the same samples used in CLIP for total RNA-seq and measured starting transcript abundance, which permitted normalization to account for differences in RNA abundance (**Table S1**).

To define the targets of hnRNP H, we first focused the analysis on the WT_SAL (wild-types treated with saline) condition. Specific hnRNP H sites were identified using Peakcaller subcommand in CLAM (Zhang and Xing, 2017) to perform peak calling throughout the whole genome. The peak calling process was done on a gene-by-gene basis by breaking down each gene into 100 nucleotide bins and looking for enrichment of mapped reads over control (or total RNA-seq mapped reads) and specifying a negative-binomial model on observed read counts. Importantly, CLAM calls peaks using the combination of uniquely- and multi-mapped reads for inclusion of RNA binding sites that are repetitive elements (Zhang and Xing, 2017). hnRNP H-associated peaks were defined as enriched ($p < 0.05$ and peak signal intensity > 1.5) in CLIP samples over input RNA-seq samples. Analysis of the peaks across gene subregions revealed enriched intronic binding of hnRNP H, comprising about 70% of total distribution (**Figure 1C**). This finding is consistent with previous characterization of hnRNP H in HeLa cells (Huelga et al., 2012; Uren et al., 2016), supporting successful isolation of hnRNP H-bound RNAs in mouse striatal tissue.

De novo motif discovery of significant hnRNP H-associated binding sites using the Homer database (Heinz et al., 2010) detected the top over-represented motif to be G-rich (**Figure 1D**) and was more prevalent in intronic regions (**Table S2**) which is in agreement with the prior literature (Lefave et al., 2011; Uren et al., 2016) and indicates that our CLIP procedure has successfully isolated of hnRNP H-associated targets in mouse brain striatal tissue. Intronic poly G-stretches can enhance hnRNP H binding (Han et al., 2005) and their length predicts splicing (Katz et al., 2010). Pathway enrichment analysis of the hnRNP H RNA targets containing these G-rich genomic locations identified “presynaptic depolarization and calcium channel opening,” comprising of subunits of calcium channels encoded by *Cacna1a, Cacnb4, Cacna1e, Cacng4, Cacna1b, Cacng2, and Cacnb2* (**Figure 1E**), all of which are important for neurotransmission (Dolphin and Lee, 2020). Another RBP that binds to mRNA transcripts that encode for ion channels is FMRP (Darnell et al., 2011). Our findings implicate hnRNP H as another RBP that binds to calcium channel subunit transcripts to regulate gene splicing and expression that likely affects neurotransmission.

hnRNP H regulates gene networks important for synaptic function

To determine whether hnRNP H regulates a subset of targets in the striatum, pathway and gene ontologies (**GO**) analyses were performed to examine the biological and molecular functions of hnRNP H targets (these targets are provided in**Table S3**). The enriched gene sets are organized into an enrichment map network (**Figure S3)**. These gene sets are connected depending on the number of shared genes where highly related gene sets are clustered together. The enrichment map network clearly revealed gene sets related to synaptic functions (**Figure S3**). The top five enriched gene sets include “transmission across chemical

synapse", "neuronal system", "axon guidance", "muscle contraction", and "mRNA processing" (*nodes, **Figure S3**). Thus, hnRNP H regulates pre-mRNAs and mRNAs encoding for proteins involved in synaptic function.

Hnrnph1 **mutation and methamphetamine treatment induce changes in RNA-binding targets of hnRNP H**

To test the hypothesis that hnRNP H exhibits a functional response to methamphetamine treatment (i.e., change its targetome), we examined the baseline and methamphetamine-induced targetome of hnRNP H in *Hnrnph1* mutants versus wild-types. Comparing changes in binding across subregions of the mRNA transcripts will tell us the extent to which the *Hnrnph1* mutation and methamphetamine impact splicing function versus mRNA stability and/or translation.

In using the 2 x 2 design (Genotype x Treatment) to analyze the read distribution separately across the 3'UTR, introns, CDS, and 5'UTR for each of the four conditions, we again discovered over-representation of binding sites for intronic regions of the mRNA transcripts across all four conditions (**Figure 2A**). In comparison to the hnRNP H binding targets at baseline (WT_SAL), changes in hnRNP H binding at 3'UTR and introns as a function of Genotype and Treatment were more variable compared to binding in the CDS and 5'UTR than would be expected by chance (**Table S4**). Thus, methamphetamine entry induced a signaling response that ultimately shifted the binding of hnRNP H to its intronic targets that is predicted to disrupt mRNA splicing. Following methamphetamine, wild-types showed an *increase* in the percentage of 3'UTR binding sites whereas *Hnrnph1* mutants showed a *decrease* in the percentage of 3'UTR binding sites. This result suggests that methamphetamine-induced intracellular signaling alters hnRNP H-mediated regulation of mRNA stability, polyadenylation site usage, and translation.

Opposing methamphetamine-induced changes in the 3'UTR targetome between *Hnrnph1* mutants versus wild-types prompted further examination. Plotting changes in hnRNP H-associated CLIP peaks in each of the four groups (Genotype x Treatment), we found that hnRNP H CLIP peaks showing methamphetamine-induced *increased* binding in wild-types were more likely to show methamphetamine-induced *decreased* binding in *Hnrnph1* mutants (**Figure 2B**). This negative correlation potentially indicates that the heterozygous *Hnrnph1* mutation exerts a dominant negative effect on hnRNP H1 function, especially in response to methamphetamine. Thus, the hnRNP H shift in binding is generally in the opposite direction between the two genotypes in response to methamphetamine (**Figure 2B**,).

Our CLIP-seq dataset identified more than 1000 mRNAs transcripts underlying Genotype and methamphetamine effects (**Figure S4A-B**). To narrow the list to those that are most relevant to genotypic differences in methamphetamine-induced dopamine release and behavior, we focused specifically on targets showing a Genotype x Treatment interaction. These targets were enriched for pathways associated with psychostimulant-induced synaptic plasticity including "amphetamine addiction," "long-term potentiation," and "dopaminergic synapse" (**Figure 2C**). The targets were found to be in cellular components of "ATPase

complex", "myelin sheath," "neuron spine", and "nuclear chromatin", all of which are involved in the cellular adaptations underlying methamphetamine exposure (**Figure 2D**). Furthermore, the enrichment map network of top over-represented pathways and GO terms for these targets revealed clustering of nodes associated with synaptic function (**Figure S4C**). Post-transcriptional regulation of these mRNA targets by hnRNP H could contribute to reduced methamphetamine-induced dopamine release in *Hnrnph1* mutants.

3'UTR and intronic targets of hnRNP H show enrichment for excitatory and psychostimulant-induced synaptic plasticity

Both genotype and methamphetamine treatment modulate *Hnrnph1* binding events within the intron and 3'UTRs (**Figure 2A**). We reasoned that those targets showing Genotype x Treatment interactions in hnRNP H binding are potential mechanistic targets that warrant further investigation. We partitioned the hnRNP H-interactive CLIP peaks into separate subgenic regions (5'UTR, 3'UTR, intron, or CDS), which allowed us to characterize the impact of changes in binding on specific types of hnRNP H-dependent post-transcriptional processing that could refine which subgenic targets are most relevant in driving the enrichment scores related to synaptic function.

We examined binding of hnRNP H across transcripts by plotting normalized $\log_2$CPM (counts per million) mapped reads to subgenic regions (**Figure 3**). We observed an opposing pattern of methamphetamine-induced changes in hnRNP H binding to 3'UTR targets between *Hnrnph1* mutants and wild-types whereby wild-types showed an increase in hnRNP H binding to the 3'UTR whereas mutants showed a decrease in hnRNP H binding to the 3'UTR. This negative correlation between methamphetamine treatment and binding was also observed for the 5'UTR, CDS, and introns (**Figure S5**) but was most pronounced for the most robust 3'UTR targets (**Figure 3**).

To gain additional mechanistic insight into the 3'UTR targets showing a Genotype x Treatment interaction in binding, KEGG enrichment analysis of subgenic regions revealed that only the 3'UTR targets showed significant enrichment for pathways associated with psychostimulant-induced synaptic plasticity (**Table 1**), Some of these 3'UTR targets, including *Gnas, Prkcb, Gria2, Grin2a,* and *Calm2* are involved in "dopaminergic synapse" and other 3'UTR targets including *Atp6v1b2, Atp60C, Slc6a1, Slc1a3, and Slc1a2* are involved in "synaptic vesicle cycling." Once again, closer examination of these enriched targets revealed opposing changes in hnRNP H binding as a function of Genotype and methamphetamine treatment. Binding of RBPs to 3'UTRs of transcripts provides a rapid means for mRNA translation at sites distance from the cell body such as the synapse (Harvey et al., 2018; Mayr, 2017). Thus, in response to methamphetamine, hnRNP H has the potential to rapidly regulate translation of proteins involved in synaptic function via changes in 3'UTR binding to mRNA transcripts. Intronic targets also showed very similar enriched pathways as those found for 3'UTR targets, thus implicating hnRNP H in splicing of transcripts coding for proteins involved in synaptic function as well (**Table 2**).

***Cacna2d2* is a methamphetamine-induced binding target of hnRNP H that is differentially regulated at the whole transcript and exon levels in *Hnrnph1* mutants versus wild-types**

We next sought to determine functional consequences of change in binding on mRNA transcript levels. To integrate striatal hnRNP H binding with gene expression and alternative splicing, we analyzed the transcriptome of striatal tissue from the same samples used in CLIP-seq. We performed both gene- and exon/intron-level transcriptome analyses to identify differentially expressed genes (**Table S5**) and genes showing evidence for alternative splicing, namely genes showing significant differential exon or intron usage (**Table S6**). *Cacna2d2* was the only gene that was identified in the analyses: 1) a binding target of hnRNP H; 2) a differentially expressed gene (Genotype x Treatment); and 3) a gene demonstrating differential exon/intron usage (Genotype x Treatment; **Figure 4A**). *Cacna2d2* showed a methamphetamine-induced increase in expression in *Hnrnph1* mutants and a methamphetamine-induced decrease in wild-types (**Figure 4B**). A total of 19 genes showed a Genotype x Treatment interaction in differential gene expression (**Figure 4B**) with 6 of them (including *Cacna2d2*) overlapping with hnRNP H targets identified in CLIP-seq (circled in **Figure 4B** and listed in **Table S7**) – a 30% overlap in binding targets and differential expression is much greater than would be expected by chance (Fisher's exact test p = 6.11E-08). One of these 6 genes was the long noncoding RNA *Malat1* which is involved in synapse formation and synaptic transmission (Zhang et al., 2017). Interestingly, multiple studies demonstrated that hnRNP H binds to *Malat1* (Arun et al., 2020; Scherer et al., 2020; Uren et al., 2016). We previously identified a trans-eQTL for *Malat1* that originates within the *Hnrnph1* behavioral QTL for reduced MA-induced locomotor activity (Yazdani et al., 2015). Other overlapping hnRNP H targets showing differential expression include *Mir124*, *Gtf2e2*, *Unc13*, and *Camta1* (**Figures 4A-B**).

Cacna2d2 codes for the voltage-dependent calcium channel subunit $\alpha 2\delta 2$. Our CLIP analysis shows that hnRNP H binds to the 3'UTR of *Cacna2d2* and thus could plausibly regulate polyadenylation site selection, mRNA stability at the 3'UTR, and ultimately CACNA2D2 protein levels (**Figure 4C**). Three putative isoforms, harboring different 3'UTR lengths, have been annotated by GENCODE. The MEME suite tools (Bailey et al., 2009) identified G-rich motifs (canonical for hnRNP H) within the 3'UTR of *Cacna2d2* (**Figure 4D**). Correspondingly, we detected alternate usage at the 3'UTR as revealed by a Genotype x Treatment Interaction ($\log_2$FC = -1.37, p = 0.033). For wild-types, decreased methamphetamine-induced hnRNP H binding was associated with increased 3'UTR usage and decreased *Cacna2d2* expression (**Figure 4E**). However, in *Hnrnph1* mutants, increased binding of hnRNP H was associated with decreased 3'UTR usage and increase in *Cacna2d2* expression (**Figure 4E**).

To further examine the opposing changes in *Cacna2d2* 3'UTR usage, using primers designed to detect differential 3'UTR usage of *Cacna2d2* (**Figure 5A**), there was a methamphetamine-induced decrease in usage of the distal end of 3'UTR of *Cacna2d2* in *Hnrnph1* mutants, with no significant change observed in wild-types (right most panel, **Figure 5B**). Notably, this distal region in *Cacna2d2* is the binding site for hnRNP H according to our CLIP-seq analysis (**Figure 4C**). Immunoblotting of the same samples as in **Figure 5B** revealed no significant change in CACNA2D2 protein after methamphetamine treatment relative to saline in the

wild-types and *Hnrnph1* mutants (**Figures 5C and S7**). A putative model of the methamphetamine-induced change in hnRNP H-*Cacna2d2* interaction at the 3'UTR in is shown in **Figure 5D**. *We propose that*, binding of hnRNP H to the distal end the 3'UTR of *Cacna2d2* prevents usage of the nearby polyadenylation site. In fact, alternative polyadenylation is a common RNA processing event through which RBPs regulate post-transcriptional control of gene expression (Batra et al., 2015; Dassi, 2017).

DISCUSSION

In this study, we defined the genome-wide hnRNP H targetome *in vivo* in the mouse striatum at baseline and the dynamic hnRNP H targetome in response to methamphetamine treatment. Furthermore, we identified the main effect of an *Hnrnph1* mutation (associated with reduced methamphetamine-induced dopamine release and behavior) on this targetome at baseline and its interactive effect on the dynamic targetome in response to methamphetamine. Most of the striatal hnRNP H targets were enriched for pathways and biological functions critical for excitatory synaptic transmission and psychostimulant addiction (**Figures S3**). The mRNAs bound by an RBP are often functionally related because these mRNAs shared sequence elements that are recognized by a given RBP and thus, are post-transcriptionally regulated as a group (Keene and Tenenbaum, 2002). For hnRNP H, the core motifs in most target mRNAs are G-rich sequences (**Figure 1D**), consistent with previous characterization of hnRNP H binding sites (Huelga et al., 2012; Lefave et al., 2011; Russo et al., 2010; Uren et al., 2016). Interestingly, most target mRNAs containing these G-rich motifs code for subunits of pre-synaptic calcium channels (**Figure 2E**). Several of the 3'UTR targets are involved in psychostimulant-induced post-synaptic excitatory plasticity and pre-synaptic neurotransmitter release (**Table 1**). Furthermore, these 3'UTR targets showed opposite methamphetamine-induced changes in hnRNP H binding between *Hnrnph1* mutants (decreased 3'UTR binding) compared to wild-types (increased 3'UTR binding) (**Figure S6**). The potential regulation of protein levels by hnRNP H binding to 3'UTR targets (e.g., regulation of repression, stability via differential 3'UTR usage, etc.) warrants future proteomic investigation. Together, CLIP-seq analysis reveals opposing methamphetamine-induced changes in hnRNP H binding of synaptic targets, depending on *Hnrnph1* genotype. The opposing methamphetamine-induced hnRNP H mRNA targetome could reflect rapidly regulated proteins that contribute to reduced methamphetamine-induced dopamine and behavior in *Hnrnph1* mutants (Ruan et al., 2020a; Yazdani et al., 2015) or they could reflect adaptive plasticity underlying differences in locomotor sensitization that depend on *Hnrnph1* genotype (Ruan et al., 2020b, 2020a).

hnRNP H is primarily localized to the nucleus of neurons in adult mice (Van Dusen et al., 2010; Kamma et al., 1995; Ruan et al., 2020a) and more recent studies have detected low levels of hnRNP H in the cytoplasm (Wall et al., 2020). It has been known that nuclear binding of RBPs to 3'UTRs can guide the cytoplasmic localization and translation of mRNA transcripts (Guramrit et al., 2015). Thus, binding of hnRNP H to 3'UTRs of mRNAs in the nucleus could recruit other proteins necessary for export of mRNAs to the cytoplasm where they are translated. We previously discovered that although *Hnrnph1* mutants showed no change in hnRNP H protein at the total striatal tissue level, they showed a robust, two-fold increase in hnRNP H protein in the striatal synaptosomal fractionation (Ruan et al., 2020a). In this study, *Hnrnph1* mutants showed extensive differences in overall RNA binding in total striatum (**Figure 2**). Thus, differential binding of hnRNP H to its synaptic targets between genotypes could be explained by the increase in synaptic hnRNP H in *Hnrnph1* mutants (Ruan et al., 2020a) which would explain the genotype-dependent enrichment of RNA-binding targets related to synaptic function as a mechanistic link, in particular with regards to the 3'UTR

targetome (**Figure 2**). Our study demonstrates rapid plasticity of the hnRNP H targetome whereby acute methamphetamine acting on presynaptic terminals and synaptic vesicles can induce rapid changes in binding of hnRNP H to mRNAs. Several RBPs have been shown to differentially alter their RNA-binding activity in response to arsenite-induced cellular stress, with distinct stress-induced interactomes in the nucleus versus the cytoplasm (Backlund et al., 2020). Much like these stress-responsive RBPs identified *in vitro*, hnRNP H also showed differential RNA binding to its targets in response to methamphetamine treatment *in vivo.*

In agreement with previous studies (Huelga et al., 2012; Uren et al., 2016), our CLIP analysis of hnRNP H identified thousands of RNA-binding targets. A major challenge is to narrow the list of functional targets that could contribute to decreased methamphetamine-induced dopamine release and behaviors in *Hnrnph1* mutants. Parallel transcriptome and spliceome analysis of the same CLIP samples permits functional interrogation of RNA-binding (Chen and Keleş, 2020; Hwang et al., 2020; Li et al., 2020) that could modulate cell biological function in response to methamphetamine. We triangulated on the methamphetamine-induced hnRNP H targetome, transcriptome, and spliceome (**Figure 4**) to identify functional links between differential hnRNP H binding and transcriptional regulation as it relates to the neurobehavioral phenotype of *Hnrnph1* mutants. *Cacna2d2* emerged as an interesting regulatory target of hnRNP H that showed a methamphetamine-induced decrease in binding and usage of the 3'UTR and an increase in *Cacna2d2* transcript in *Hnrnph1* mutants (**Figure 4E**). *Cacna2d2* is expressed in the cerebellum, striatum, and hippocampus (Dolphin, 2012), and codes for a pre-protein that is proteolytically processed into $\alpha2$ and $\delta2$ subunits of voltage-gated calcium channels (**VGCCs**) (Dolphin and Lee, 2020). These $\alpha2\delta2$ subunits localize VGCCs to the active zone and promote neurotransmitter release (Dolphin, 2013). Overexpression of $\alpha2\delta2$ subunits decreased presynaptic calcium elevation in response to an action potential, yet somehow increased vesicular release (Hoppa et al., 2012). In addition, overexpression of *Cacna2d2* disrupted intracellular calcium signaling and mitochondrial function (Carboni et al., 2003). Changes in intracellular calcium are tightly linked to changes in mitochondrial function as mitochondria can serve to buffer intracellular calcium levels (Rizzuto et al., 2012). Our previous proteomic analysis of the striatal synaptosome showed opposite changes in mitochondrial protein levels compared in *Hnrnph1* mutants versus wild-types following methamphetamine administration (Ruan et al., 2020a). Acutely, methamphetamine can inhibit calcium entry into L-type and N-type VGCCs, with longer exposure leading to a compensatory upregulation of *Cacna1c* transcript levels in SH-SY5Y cells (Andres et al., 2015). Both intracellular and extracellular calcium contribute to methamphetamine-induced dopamine release in the ventral striatum (Yorgason et al., 2020). Our identification of *Cacna2d2* dynamics at multiple levels of analysis following methamphetamine administration (3'UTR binding, transcription, and splicing) suggests that regulation of this calcium channel subunit and others (**Figure 1E**) could comprise a rapid, adaptive means for regulating calcium entry and mitigating the salient cell biological effects of methamphetamine. Notably, dopamine transporter and vesicular monoamine transporter, the two molecular targets of methamphetamine that increase the extracellular level of dopamine at the synapse (Fleckenstein and Hanson, 2003; Siciliano et al., 2014), were not identified as RNA-binding targets of hnRNP H, indicating that hnRNP H does not rapidly modulate their RNA fate.

The precise roles of RBPs in methamphetamine-induced synaptic plasticity are largely unexplored. The hnRNP H striatal targetome we have described is positioned to regulate excitatory and psychostimulant synaptic plasticity. Similarly, the targetome of FMRP (another RBP implicated in psychostimulant behavior; Smith et al., 2014) also revealed targets linked to synaptic function (Darnell et al., 2011). Dynamic regulation of synaptic protein synthesis following activation of neurotransmitter receptors, plays a key role in synaptic plasticity (Bramham and Wells, 2007). FMRP localizes to dendrites to regulate mRNA transport and synaptic plasticity (Bassell and Warren, 2008). Stimulation of metabotropic glutamate receptors in primary neuronal culture can rapidly dephosphorylate FMRP, leading to a dissociation of FMRP from miR-125a and translational activation of PSD-95 mRNA (Muddashetty et al., 2011). D1 dopamine receptor activation in prefrontal cortical neurons results in phosphorylation of FMRP and synthesis of synaptic proteins needed for glutamate receptor trafficking (Wang et al., 2008, 2010). Thus, phosphorylation of an RBP can affect translational regulation in response to receptor activation. We previously reported that treatment with a D1 dopamine receptor agonist (but not a D2 agonist) in cultured rat primary cortical neurons induced a D1 antagonist-reversible increase in nuclear immunocytochemical staining of hnRNP H without altering nuclear protein levels (Ruan et al., 2018), suggesting a potential post-translational modification of hnRNP H and/or its protein/RNA complexes. Thus, the methamphetamine-induced hnRNP H striatal targetome could plausibly be regulated by post-synaptic D1 dopamine receptor signaling and post-translational modifications of hnRNP H that in turn modulate RNA-binding and the production of proteins underlying excitatory synaptic plasticity.

To summarize, we provide the first methamphetamine-induced RNA targetome study of an RBP in the striatum. Analysis of drug-induced RBP targetomes, especially for drugs of abuse, is a novel, yet understudied approach for understanding rapid, synaptic gene regulation as it relates to cell biological adaptations in neuronal excitability, neurotransmitter release, synaptic plasticity, and behavior. We focused on hnRNP H, given the evidence for its role in methamphetamine-induced dopamine release and behavior (Bryant and Yazdani, 2016; Ruan et al., 2020b, 2020a; Yazdani et al., 2015). We established hnRNP H as a novel gene regulatory link among several target mRNAs coding for proteins that are well-established to mediate psychostimulant-induced neurotransmission and plasticity. Our study design represents a powerful approach for integrating complementary gene sets from different “omic” methods (interactome, transcriptome, and spliceome) that can be broadly applied to the study of drug-induced RBP-RNA dynamics and discovery of functionally relevant RNA-binding targets underlying cell biological responses, adaptations, and organismal phenotypes such as behavioral disorders.

FIGURE LEGENDS

Figure 1. RNA-binding sites of hnRNP H at baseline in saline control wild-types are enriched for introns and G-rich binding motifs. eCLIP-seq revealed transcriptome-wide striatal RNA targets associated with hnRNP H in saline control wild-types (WT_SAL). Peak calling of both uniquely and multi-mapped reads was performed using CLAM (Zhang and Xing, 2017). **(A):** Acute methamphetamine-induced locomotor activity on Day 3 for 30 min in 5-min bins. Thirty min post methamphetamine (MA) injection, mice were sacrificed and whole striatum from each mouse was dissected and harvested for CLIP-seq processing. *Hnrnph1* mutants (MUT) showed less locomotor activity compared to wild-types [$F(5,280)_{\text{Genotype x Treatment x Time}} = 7.354$, p = 1.70e-06]. In considering the time-course of locomotor activity following methamphetamine, there was a significant decrease in total distance traveled in *Hnrnph1* mutants relative to wild-types in response to saline on Day 3 at 0 – 5 min bin F(1,30) = 6.687, $^{\%}p = 0.015$; and a significant decrease in distance traveled in *Hnrnph1* mutants relative to wild-types following methamphetamine on Day 3 at 10 – 15 min bin [F(1,30) = 5.163, *p =0.030, 15 – 20 min bin [F(1,30) = 5.259, *p = 0.029], 20 – 25 min bin [F(1,30) = 5.187, *p = 0.030], and 25 – 30 min bin [F(1,30) = 5.895, *p = 0.021]. No effect of Sex or interaction of Sex with other factors was detected for any of the measure reported. n = 8 per Sex per Genotype per Treatment. No difference in locomotor activity was found in response to saline on Days 1 and 2 (**Figure S2**). **(B):** CLIP and ^{32}P labeling of hnRNP H-bound RNA. CLIP conditions are shown for each lane: no crosslinking, IgG mock IP, and four different RNase I_f concentrations from high to low. An increasing amount of RNA was pulled down as the concentration of RNase I_f was decreased. The scissors denote the region above the molecular weight of hnRNP H (50 kDa) that was isolated for sequencing. The region runs from 50 to 80 kDa, which corresponds to 30 to 70 bp for RNA length. The larger bands observed above 100 kDa could represent very long RNAs that are resistant to digestion or large hnRNP H-associated protein-protein complexes bound to RNAs. **(C):** hnRNP H binds primarily to introns of target RNAs. More than 70% of hnRNP H CLIP sites are intronic. The pie chart shows the relative distribution of CLIP sites in 5'UTR, coding sequences (**CDS**), introns, and 3'UTR. Proximal introns indicate less than 200 (proximalx200_intron) or 500 (proximalx500_intron) nucleotides from the 5' or 3' splice sites with the remainder annotated as distal introns. Unannotated exons are referred to as "other exons". **(D):** Poly-G tract is the most prevalent component of the hnRNP H binding motif. *De novo* motif discovery of hnRNP H CLIP sites was performed using Homer (Heinz et al., 2010). **(E):** hnRNP H RNA-binding targets containing G-rich motifs in their binding sites are most highly enriched for "presynaptic depolarization and calcium channel opening" pathway. Pathway enrichment analysis of hnRNP H RNA-binding targets with the poly-G motif was performed in WebGestalt (Liao et al., 2019) using the over-representation analysis methods. The top 10 pathways with FDR > 0.05 are shown, sorted from high to low enrichment ratio.

Figure 2. RNA-binding targets of hnRNP H showing a Genotype x Treatment interaction are enriched for pathways and cellular components involved in drug-evoked synaptic plasticity. eCLIP-seq analysis revealed transcriptome-wide striatal RNA-binding targets associated with hnRNP H in untreated saline or methamphetamine-treated *Hnrnph1* mutants versus wild-types. Peak calling in CLAM (Zhang and Xing, 2017) was performed separately for each of the four conditions. For differential analysis, peak calling was also performed using CLAM (Zhang and Xing, 2017) on the merged bam file across all conditions followed by read counts against the identified peaks and differential analysis of peak intensity. WT_SAL = untreated saline wild-types; WT_MA = methamphetamine-treated wild-types; MUT_SAL = untreated saline *Hnrnph1* mutants; MUT_MA = methamphetamine-treated *Hnrnph1* mutants. **(A):** In comparison to WT_SAL, only the percentages of hnRNP H binding events associated with 3'UTR and introns were significantly different in the other three conditions (See chi-square tests in **Table S4**). The percentage that comprised 3'UTRs varied between Genotype and Treatment: an increase in response to methamphetamine in wild-types compared to their saline-treated wild-type counterparts; a decrease following methamphetamine in *Hnrnph1* mutants compared to their saline-treated mutant counterparts (chi-square test: *$p < 0.001$). All intron binding events (including distal introns and proximal introns) were significantly different from saline-treated wild-types (chi-square test: all p's < 0.001, with the exception of saline-treated *Hnrnph1* mutants ($p = 0.453$ for proximalx200_intron). The relative distribution of RNA- binding sites over the gene elements for each of the four conditions in the 2 x 2 (Genotype x Treatment) experimental design is shown. **(B):** An hnRNP H CLIP peak with increased binding in wild-types in response to methamphetamine is more likely to show decreased binding in *Hnrnph1* mutants. The plot shows a negative correlation between $\log_2$FC(WT_MA vs WT_SAL) and $\log_2$FC(MUT_MA vs MUT_SAL) (Pearson's correlation coefficient $r = -0.034$, $p < 2.2e-16$). The hnRNP H CLIP peaks showing Genotype x Treatment interactions (highlighted in magenta) showed a much stronger negative correlation (Pearson's $r = -0.692$, $p < 2.2e-16$). Each data point corresponds with a hnRNP H-associated CLIP peak. **(C):** Strong enrichment scores for "amphetamine addiction", "alcoholism", "long-term potentiation", and "dopaminergic synapse" pathways were detected for those hnRNP H RNA-binding targets showing Genotype x Treatment interaction. GSEA analysis was performed in WebGestalt (Liao et al., 2019) on a ranked list (based on $\log_2$FC) of hnRNP H targets showing Genotype x Treatment interaction. **(D):** Strong enrichment for "ATPase complex", "myelin sheath", "neuron spine" and "nuclear chromatin" cellular components were detected for those hnRNP H RNA-binding targets showing Genotype x Treatment interaction.

Figure 3. 3'UTR targets showed opposite changes in methamphetamine-induced binding to hnRNP H between *Hnrnph1* mutants and wild-types. Genotype x Treatment-associated hnRNP H CLIP peaks, divided into 4 gene elements: 5'UTR, 3'UTR, intron, and CDS. Heatmaps show normalized $\log_2$CPM (count-per-million) read counts for significant peaks demonstrating a Genotype x Treatment interaction. The interaction is expressed as (MUT_MA – MUT_SAL) – (WT_MA – WT_SAL). The row of each heatmap represents a binding site sorted by p value from smallest to largest, where those with a p-value of less than 0.01 are shown in the heatmap. Saline control *Hnrnph1* mutants show an increase in baseline binding of hnRNP H to the 3'UTR regions of RNA-binding targets that decreases in response to methamphetamine treatment. WT_SAL =

untreated saline wild-types; WT_MA = methamphetamine-treated wild-types; MUT_SAL = untreated saline *Hnrnph1* mutants; MUT_MA = methamphetamine-treated *Hnrnph1* mutants.

Figure 4. *Cacna2d2* is the one convergent RNA target showing a Genotype x Treatment-induced change in hnRNP H1 binding, gene expression, and alternative splicing. Differential gene expression (DE) for the interaction of Genotype and Treatment [(MUT_MA – MUT_SAL) – (WT_MA – WT_SAL)] was performed using limma (Ritchie et al., 2015) and edgeR (Robinson et al., 2009). Differential exon and intron usage analysis (alternatively spliced; AS) for interaction of Genotype and Treatment [(MUT_MA – MUT_SAL) – (WT_MA – WT_SAL)] was performed using Aspli (Mancini et al., 2020). **(A):** Venn diagram comparing RNA-binding targets of hnRNP H with differential gene expression and differential exon or intron usage. The 19 DE genes and 469 AS genes were then compared with the hnRNP H targets that comprised the Genotype x Treatment interactions. *Cacna2d2* is the only RNA-binding target of hnRNP H that was both a DE gene and an AS gene. Only the top overlapping and non-overlapping hnRNP H targets and AS genes are indicated. Out of the 19 DE genes, *Cacna2d2, Elfn1*, *Calb2*, and *Zic1* are putative targets of *Malat1* (predicted by TargetScan; Agarwal et al., 2015) while *Camta1* and *Pcdh8* are putative targets of *Mir124a* (predicted by LncRRIsearch; Fukunaga et al., 2019) . **(B):** Volcano plot of genes showing a Genotype x Treatment interaction in response to methamphetamine. The interaction is expressed as (MUT_MA – MUT_SAL) – (WT_MA – WT_SAL). *Cacna2d2* is circled in red. The five overlapping hnRNP H targets and DE genes are circled in purple. **(C):** hnRNP H preferentially binds to the 3'UTR of *Cacna2d2*. Visualization of reads by Integrative Genome Browser (Thorvaldsdóttir et al., 2013) for the hnRNP CLIP peak at the 3'UTR of *Cacna2d2*. Scale of the plot height is in counts per million (CPM). **(D):** A G-rich motif was detected at the hnRNP H CLIP peak within the 3'UTR of *Cacna2d2*. *De novo* motif discovery of the binding site was performed in MEME (Bailey et al., 2009). **(E):** Interaction plots showing hnRNP H binding to the 3 'UTR of *Cacna2d2* (left), differential usage of the 3'UTR (middle), and differential gene expression of *Cacna2d2* (right) as a function of Genotype and Treatment. The increase in hnRNP H binding to the 3'UTR of *Cacna2d2* was associated with decreased 3'UTR usage and increased gene expression *of Cacna2d2* in *Hnrnph1* mutants. Here, 3'UTR usage is defined as to the number of normalized reads mapped to the 3'UTR portion of *Cacna2d2*. The interaction plots were generated from CLIP-seq and RNA-seq data showing average values with standard deviation of the means, with n = 3 per condition.

Figure 5. RT-qPCR analysis detected a decreased usage of the distal end of the 3'UTR of *Cacna2d2* (also the binding site for hnRHP H) in *Hnrnph1* mutants in response to methamphetamine. CLIP-seq analysis identified an increase in hnRNP H binding to the distal end of 3'UTR of *Cacna2d2* in *Hnrnph1* mutants that was associated with decreased usage of the 3'UTR, warranting further validation. **(A):** Three polyadenylation sites (pA-1, pA-2, and pA-3) are present within the 3'UTR of *Cacna2d2* that distinguish isoforms containing 3'UTR of different lengths (UCSC genome browser). Primers were designed to detect difference in usage of the proximal and distal end of the 3'UTR of *Cacna2d2* as well as exons 37-38 and exons

3-4. The schematic indicates the positions of these primers. SAL = saline; MA = methamphetamine; WT = wild-types; H1 MUT = *Hnrnph1* mutants. **(B):** The left striata were harvested from mice in the same way as in CLIP-seq followed by RNA extraction, cDNA library generation with oligo-DT primers, and RT-qPCR to detect differential usage of the regions at the 3'UTR of *Cacna2d2* and upstream of it. No differences were found at exons 3-4 [$F(1,39)_{Genotype\ x\ Treatment} = 0.650$, $p = 0.425$], exons 37-38 [$F(1,39)_{Genotype\ x\ Treatment} = 0.900$, $p = 0.349$], or at the proximal end of the 3'UTR [$F(1,39)_{Genotype\ x\ Treatment} = 0.198$, $p = 0.659$]. Although no significant Genotype x Treatment interaction was detected for the usage of the distal end of the 3'UTR [$F(1,39)_{Genotype\ x\ Treatment} = 1.485$, $p = 0.230$], there was a significant main effect of Treatment [$F(1,39)_{Treatment} = 10.772$, $p = 0.002$]. In examining the effect of Treatment at each level of Genotype, a significant, simple main effect of Treatment was found in the *Hnrnph1* mutants [$F(1,40)_{Treatment} = 9.368$, $p = 0.004$] but not in the wild-types [$F(1,40)_{Treatment} = 2.993$, $p = 0.091$]. Subsequent analysis revealed decreased methamphetamine-induced usage of the distal end of 3'UTR in *Hnrnph1* mutants compared to wild-types [$t(40) = -3.061$, $*p = 0.004$], with no significant genotypic difference between saline groups [$t(40) = -1.730$, $p = 0.091$]. The normalized $2^{-\Delta\Delta CT}$ values from three independent replicates are shown in the plots. **(C):** The right striata of the same mice from the RT-qPCR analysis (Figure 5B) were collected for Western blot analysis to assess differences in CACNA2D2 protein expression. Immunoblots from three separate replicates are shown on the left with quantification shown on the right. There was no significant genotypic difference in the level of CACNA2D2 protein in saline or methamphetamine treatment groups [$F(1,40)_{Genotype\ x\ Treatment} = 2.587$, $p = 0.117$]. **(D):** Schematics showing the putative interaction between hnRNP H-mediated selection of polyadenylation site in *Cacna2d2.* We proposed that binding of hnRNP H to the pA-3 site within the 3'UTR of *Cacna2d2* blocks the usage of pA-3 to produce transcripts with a shorter 3'UTR in *Hnrnph1* mutants in response to methamphetamine, (shown on right). This observation was identified in alternative splicing analysis (Figure 4E, middle panel) and subsequently validated in the RT-qPCR (Figure 5B, rightmost panel).

STAR Methods

Key Resources Table

REAGENT or RESOURCE	SOURCE	IDENTIFIER
Antibodies		
Anti-CACNA2D2 ($Ca_V\alpha2\delta2$) (extracellular) Antibody	alomone labs	Cat#ACC-102
Peroxidase-AffiniPure Donkey Anti-Rabbit IgG (H+L) antibody	Jackson ImmunoResearch Labs	Cat#711-035-152; RRID: AB_10015282
Deposited Data		
CLIP-seq raw and processed data	This paper	GEO: GSE160682
RNA-seq raw and processed data	This paper	GEO: GSE160682
Experimental Models: Organisms/Strains		

Mouse: H1_Mut: C57BL/6J-*Hnrnph1*^{em1Lagbu}/J	The Jackson Laboratory	Cat#JAX:033968; RRID: IMSR_JAX:033968
Oligonucleotides		
Proximal end of the 3'UTR of *Cacna2d2* (forward primer)	Integrated DNA Technologies	5'-TTGGCCACTCTCTCCTGAAG-3'
Proximal end of the 3'UTR of *Cacna2d2* (reverse primer)	Integrated DNA Technologies	5'-ACTAGTGGCCTCCTGTCCTA-3'
Distal end of the 3'UTR of *Cacna2d2* (forward primer)	Integrated DNA Technologies	5'-CCCCATCAGGTAGTTGTCCA-3'
Distal end of the 3'UTR of *Cacna2d2* (reverse primer)	Integrated DNA Technologies	5'-TGTCGCTGTTGTTTTCCCAA-3'
Exons 37-38 of *Cacna2d2* (forward primer)	Integrated DNA Technologies	5'-GGTCCGCACATCTGTTTTGA-3'
Exons 37-38 of *Cacna2d2* (reverse primer)	Integrated DNA Technologies	5'-GAAGGAGTGGACTTGAGGCT-3'
Exons 3-4 of *Cacna2d2* (forward primer)	Integrated DNA Technologies	5'-AATTGGTGGAGAAAGTGGCA-3'
Exons 3-4 of *Cacna2d2* (reverse primer)	Integrated DNA Technologies	5'-GGCTTTCTGGAAATTCTCTGC-3'
Exons 5-6 of *Gapdh* (forward primer)	Integrated DNA Technologies	5'-GCCTTCCGTGTTCCTACC-3'
Exons 5-6 of *Gapdh* (reverse primer)	Integrated DNA Technologies	5'-CCTCAGTGTAGCCCAAGATG-3'
Software and Algorithms		
Trimmomatic	Bolger et al., 2014	http://www.usadellab.org/cms/?page=trimmomatic
UMI-tools	Smith et al., 2017	https://github.com/CGATOxford/UMI-tools
STAR	Dobin et al., 2013	https://github.com/alexdobin/STAR
BEDtools	Quinlan and Hall, 2010	https://github.com/arq5x/bedtools2
CLAM	Zhang and Xing, 2017	https://github.com/Xinglab/CLAM
Homer	Heinz et al., 2010	http://homer.ucsd.edu/homer/motif/rnaMotifs.html
g:Profiler	Raudvere et al., 2019	https://biit.cs.ut.ee/gprofiler/page/docs
Cytoscape (EnrichmentMap)	Merico et al., 2010	https://enrichmentmap.readthedocs.io/en/latest
WebGestalt	Liao et al., 2019	http://www.webgestalt.org/WebGestalt_2019_Manual.pdf
SubRead (featureCounts)	Liao et al., 2014	http://subread.sourceforge.net
R	R Core Team, 2013	https://www.r-project.org
limma (R package)	Ritchie et al., 2015	https://bioconductor.org/packages/release/bioc/html/limma.html
edgeR (R package)	Robinson et al., 2009	https://bioconductor.org/packages/release/bioc/html/edgeR.html
ASpli (R package)	Mancini et al., 2020	https://bioconductor.org/packages/release/bioc/html/ASpli.html
ImageJ	NIH	http://https://imagej.nih.gov
TargetScan	Agarwal et al., 2015	http://www.targetscan.org/vert_72

LncRRIsearch	Fukunaga et al., 2019	http://rtools.cbrc.jp/LncRRIsearch

Resource Availability

Lead Contact

Requests for resources, reagents, and any information should be directed to Camron D. Bryant (camron@bu.edu).

Materials Availability

All materials are available and they are listed in the Key Resources Table above.

Data and Code Availability

Raw and processed sequencing data from CLIP-seq and RNA-seq can be accessed through the National Center for Biotechnology Information's Gene Expression Omnibus (**GEO**) under the accession number GSE160682. Codes associated with analyses mentioned in Method Details can be found at: https://github.com/camronbryant/hnrnph1_clip

Experimental Model and Subject Details

Mice

Hnrnph1 mutants were generated via TALENs-mediated induction of a small, 16 bp deletion in the first coding exon as described (Yazdani et al., 2015) and have been deposited to The Jackson Laboratory repository (Cat#JAX033968). A two-fold increase in hnRNP H protein expression was detected in the striatal synaptosome of *Hnrnph1* mutants compared to wild-types with no change in total tissue level (Ruan et al., 2020a). Mice were generated by mating heterozygous *Hnrnph1* mutant males with C57BL/6J females purchased from The Jackson Laboratory (Cat#JAX000664), yielding offspring that were approximately 50% heterozygotes for the *Hnrnph1* mutation and 50% wild-types. Both female and male offspring (ranging from 50 – 100 days old at the start of the experiment) from this breeding scheme were used in the study and were genotyped as described (Yazdani et al., 2015). Mice were housed in same-sex groups of 2-5 in standard mouse cages in ventilated racks under standard housing conditions on a 12 h:12 h light:dark schedule with food and water supplied ad libitum. All protocols involving mice were in accordance with the Guideline for the Care and Use of Laboratory Animals and were approved by Boston University's IACUC committee.

Method Details

Methamphetamine-induced locomotor activity followed by dissection of whole striatum

As described (Yazdani et al., 2015), on Days 1 and 2, all mice received a saline injection (10 ml/kg, i.p.) and were recorded for locomotor activity in Plexiglas chambers (40 cm length x 20 cm width x 45 cm height) for 1 h.

On Day 3, mice receive either saline again or methamphetamine (2 mg/kg, i.p.; Sigma Aldrich) and were recorded for locomotor activity for 30 min and the whole striata (left and right sides) were dissected from each mouse at 30 min post-injection (Ruan et al., 2020a). Dissected whole striata were stored in RNAlater (ThermoFisher Scientific, Cat#AM7020) following manufacturer's instructions to stabilize the RNA and protein followed by cross-linking immunoprecipitation (CLIP) library preparation as described below.

CLIP

Striata from four mice were pooled per replicate (3 replicates per Genotype per Treatment). Each replicate used for CLIP-seq and RNA-seq was generated by pooling striata from 4 *Hnrnph1* mutants or 4 wild-types across multiple litters. Each pool consisted of samples from 2 females and 2 males. The striatum was chosen because of its involvement in the methamphetamine locomotor stimulant response, reinforcement and reward (Keleta and Martinez, 2012; Lominac et al., 2014). Given the large amount of striatal tissue needed for generating the CLIP-seq libraries in this study, we did not examine the ventral tegmental area (**VTA**, where the nuclei of the dopaminergic neurons reside) because the number of mice required to obtain a sufficient amount of tissue from the VTA per replicate was not feasible. The striatum punches contained primarily post-synaptic cells but they also contained presynaptic dopaminergic terminals. Thus, any low levels of cytosolic hnRNP H (Wall et al., 2020) and its bound RNAs at the presynaptic terminal were expected to be captured within the samples and thus, potentially relevant to rapid, dynamic regulation of dopamine release in response to methamphetamine. The experimental design is outlined in **Table S1**. Tissue was flash frozen in the mortar-filled liquid nitrogen and crushed into powder with the pestle and kept on dry ice in a 100 mm Petri dish until use. Prior to crosslinking, a portion of the pooled tissue from each replicate was removed and stored in -80°C for later RNA extraction and bulk RNA-seq library preparation. The tissue was kept on dry ice in the dish while crosslinking was performed for three rounds using a 400 mJ/cm^2 dosage of 254 nm ultraviolet radiation. The crosslinked tissue was then homogenized in 1 ml of lysis buffer (50 mM Tris-HCl pH7.4, 100 mM NaCl, 1% NP-40 (Igepal CA630), 0.1% SDS, 0.5% sodium deoxycholate (protect from light), protease and phosphatase inhibitor cocktail (1:100; ThermoFisher Scientific, Cat#78444) and recombinant RNasin ribonuclease inhibitor (1 ul/ml; Promega, Cat#N2511) with a mechanical homogenizer followed by addition of TURBO DNase (2 µl; ThermoFisher Scientific, Cat#AM2239). The lysate was kept on ice for 30 min followed by the addition of RNAse I_f (125 U/ml; NEB, Cat#M0243L) and was allowed to incubate in a thermomixer set to 1200 RPM at 37°C for 3 min. The lysate was then centrifuged at 20,000 x g for 20 min at 4°C and kept on ice until use.

For RNA-immunoprecipitation, 133.3 µl of MyOne Streptavidin T1 beads (Invitrogen, Cat#65602) were incubated with 5.8 µl of 1 mg/ml of Pierce™ biotinylated Protein G (ThermoFisher Scientific, Cat#29988) and 20 µg of either the hnRNP H antibody (Bethyl; Cat#A300-511A) or the rabbit IgG antibody (EMD Millipore, Cat#12-370) for 1 h. The antibody-coupled beads were washed five times with 0.5% IgG-free BSA (Jackson ImmunoResearch; Cat# 001-000-162) in 1X PBS, followed by three washes in lysis buffer. The lysate that was clarified by centrifugation was added to the coated and washed beads and incubated with end-to-end rotation

at 4°C for 2 h followed by 2X wash with 500 µl of wash buffer (end-over-end rotation at 4°C for 5 min each) and another 2X wash with 500 µl of high salt wash buffer (end-over-end rotation at 4°C for 5 min each). The components of the wash buffer are as follows: 20 mM Tris-HCl pH7.4, 10 mM $MgCl_2$, 0.2% Tween-20, and recombinant RNasin ribonuclease Inhibitor (1 uL/ml, Promega, Cat#N2511). The components of the high salt wash buffer are as follows: 50 mM Tris-HCl pH7.4, 1M NaCl, 1 mM EDTA, 1% NP-40, 0.1% SDS, 0.5% sodium deocxycholate, and recombinant RNasin ribonuclease inhibitor (1 uL/ml; Promega, Cat#N2511). These washes were followed by an additional wash with 500 µl each of both wash buffer and high salt wash buffer. Two additional final washes were performed with 500 µl of wash buffer. The rest of the wash buffer was removed and beads resuspended in 20 µl of 1X Bolt LDS non-reducing sample buffer (ThermoFisher Scientific, Cat# B0007). The beads in sample buffer were then heated at 70°C for 10 min prior to SDS-PAGE on a 4-12% gradient NuPAGE Bis/Tris gels (ThermoFisher Scientific, Cat#NP0322BOX) followed by transfer to nitrocellulose membrane (Amersham Protran Premium 0.45 NC; Cat#10600078) with 10% methanol for 6 hours at constant 150 mA.

CLIP-seq and total RNA-seq library preparation

Following the completion of membrane transfer, the membrane was cut with a clean razor to obtain a vertical membrane slice per lane from 50 kDa (molecular weight of hnRNP H) to 75 kDa, which translates to 30 to 70 nucleotide RNA fragments crosslinked to the protein. RNA was then extracted from the membrane slices following a previously described procedure (Rieger et al., 2020). The same extraction procedure (starting with the addition of 7M urea) was used to isolate RNA from samples previously stored for total RNA-seq. Following RNA extraction, sample concentration was quantified with Agilent Bioanalyzer and approximately 0.2 ng of RNA was used to prepare next-generation sequencing libraries following a published protocol for library preparation (Rieger et al., 2020). Because the RNA adapter on each sample contained a unique barcode, the cDNA libraries generated from the sample (12 CLIP-seq and 12 RNA-seq libraries) were multiplexed and pooled for increased throughput. A pooled library at a concentration of 10 nM was shipped to the University of Chicago Sequencing core and subjected to 100 bp paired-end 2 x 100 sequencing in a single lane on Illumina HiSEQ4000. To increase read coverage for the RNA-seq samples, those 12 cDNA libraries were pooled (10 nM concentration) for sequencing for a second time in one lane using Illumina HiSEQ4000. The read coverage for each sample is shown in **Table S1**.

CLIP-seq and total RNA-seq data processing

Reads were trimmed for quality using Trimmomatic (Bolger et al., 2014). Unique Molecular Identifier (UMI) sequences were extracted from Read 2 for removal of PCR amplification duplicates using the 'extract' command in UMI-tools (Smith et al., 2017). After the reads were trimmed and UMI extracted, we used STAR (Dobin et al., 2013) to map reads to mouse genome, version GRCm38/mm10. Even though the samples had undergone ribosomal RNA (rRNA) depletion prior to library preparation, we used BEDtools (Quinlan and Hall, 2010) to intersect the bam files with the RNA annotation bed file exported from UCSC Table browser

(Karolchik et al., 2004) to remove rRNAs and other repetitive RNAs. Using the 'dedup' command in UMI_tools (Smith et al., 2017), PCR duplicates from the rRNA-depleted bam files were removed based on UMI extracted in the previous step.

Peak calling using CLIP-seq Analysis of Multi-mapped reads (CLAM)

To define the binding sites for hnRNP H for each of the four conditions separately, deduplicated bam files for the three replicates of each condition were used for peak calling in CLAM (Zhang and Xing, 2017). The BAM file for the CLIP sample and the BAM file for input (corresponding RNA-seq sample) were used as input along with a gene annotation file in Gene Transfer Format downloaded from GENCODE. Following the steps described in CLAM (Zhang and Xing, 2017), in order to allow for peak calling of multi-mapped reads, BAM files were preprocessed ('preprocessor' command) first to separate multi-mapped reads and unique mapped reads followed by realigning ('realigner' command) and then peak calling ('peakcaller' command) on a gene-by-gene basis in 100-bp bins. The called peaks were then annotated to the genomic regions using the 'peak_annotator' command to examine binding site distributions across the 5'UTR, 3'UTR, CDS, and introns. The genomic region annotated peaks for each condition can be found in the supplementary files associated with GEO accession number GSE160682.

Homer *de novo* Motif Discovery

To identify the top over-represented motifs in the peaks (those peaks with CLIP peak intensity > 1.5) that were identified in CLAM, Homer software (Heinz et al., 2010) was used for *de novo* motif discovery by using "findMotifsGenome.pl" function. The input file comprised a list of hnRNP H associated peaks containing the genomic coordinates. The "annotatePeak.pl" function was then used to identify motif locations to find genes containing a particular motif.

Pathway and Gene Ontology Enrichment Analysis

To examine the biological function of the hnRNP H targets (peak signal value defined by a CLAM value greater than 1.5 for each target), we performed pathway and gene ontology (**GO**) enrichment analysis of those targets in g:Profiler (Raudvere et al., 2019) against the following data sources: Reactome, WikiPathways, GO molecular function, GO cellular component, and GO biological process. The top 10 pathways and GO terms from each these 5 databases (a list of 50 gene sets) were used for network analysis in Cytoscape using the EnrichmentMap module (Merico et al., 2010). Highly redundant gene sets were grouped together as clusters for clear visualization and easy interpretation. The same pathway and GO enrichment analyses were performed in g:Profiler for the hnRNP H targets with Genotype and Treatment interaction to generate an EnrichmentMap (Reimand et al., 2019). To to examine the biological relevance separately for each subgenic region of hnRNP H targets, we performed KEGG (Kanehisa et al., 2019) pathway enrichment analysis in WebGestalt (Liao et al., 2019).

3'UTR usage for *Cacna2d2* using real-time quantitative PCR (RT-qPCR)

Striatal tissue for RT-qPCR validation were collected 30 min after saline or methamphetamine injections as described above. The left striatum was dissected as previously described (Ruan et al., 2020a) and subsequently stored in RNAlater (ThermoFisher Scientific, Cat#AM7020) following manufacturer's instructions to stabilize the RNA. Following RNA extraction with TRIzol reagent (Invitrogen, Cat#15596026), oligo-DT primers were used to synthesize cDNA from the extracted total RNA using a high-capacity cDNA reverse transcription kit (ThermoFisher Scientific, Cat#4368814). RT-qPCR using PowerUP SYBR Green (ThermoFisher Scientific, Cat#A25741) was then performed to evaluate differential 3'UTR usage of *Cacna2d2*. The primer sequences are listed in the Key Resource Table above.

SDS-PAGE and immunoblotting for CACNA2D2 protein quantification

The right striatum from the same mice used for the RT-qPCR analysis was processed for Western blots for quantification of CACNA2D2 protein level 30 minutes after methamphetamine or saline injections in *Hnrnph1* mutants and wild-types. The flash-frozen striatal tissues were homogenized using a hand-held homogenizer in RIPA buffer which included protease and phosphatase inhibitor cocktail (1:100; ThermoFisher Scientific, Cat#78444) followed by sonication. For each sample, 30 μg of protein was heated in a 70°C water bath for 10 min prior to loading into into a 4-15% Criterion TGX precast Midi protein gel (Bio-Rad, Cat#5671094) for SDS-PAGE followed by wet transfer to a nitrocellulose membrane. Following the transfer, membranes were stained with ponceau S solution (0.1% ponceau S in 1% (v/v) acetic acid for 1 minute de-stained in water to remove non-specific binding. The membranes were then imaged with BioRad ChemiDoc XRS+ system. Following the imaging, the membranes were blocked with 5% milk for 1 hand probed with anti-CACNA2D2 (1:1000; alomone, Cat#ACC-102) over night at 4°C followed by 1 hour probing with donkey anti-rabbit HRP (1:10,000; Jackson ImmunoResearch Labs Cat#711-035-152). The membrane were imaged via enhanced chemiluminescence photodetection with the BioRad ChemiDoc XRS+ system.

Quantification and Statistical Analysis

MA-induced locomotor activity

To replicate the findings of reduced methamphetamine-induced locomotor activity in *Hnrnph1* mutants as previously observed (Ruan et al., 2020a; Yazdani et al., 2015), total distance traveled in 5-min bin separately for Days 1, 2, and 3 was analyzed using mixed effects ANOVA with Genotype, Sex, and Treatment (saline, methamphetamine) as between-subjects factors and Time as the repeated-measures factor. For Day 3, the significant three-way (Genotype x Treatment x Time) was decomposed into a simple two-way (Genotype x Treatment) interaction at each time level. The significant simple two-way interaction was then followed up with simple main effects to investigate the effect of Genotype on distance traveled at every level of time. The significant simple main effect for the methamphetamine treatment was then followed up by multiple pairwise comparisons to identify genotypic differences in each 5-min time bin.

Comparisons of Genotype and Treatment effects on hnRNP H binding site distributions

The total percentage of hnRNP H binding sites was associated with 4 subgenic regions (5'UTR, 3'UTR, CDS, and introns) as shown in **Figure 2A**. Differences in the percentage of hnRNP H associated subgenic binding regions relative to WT_SAL (wild-types treated with saline) were calculated using ch-square tests as shown in **Table S4**.

Effect of Genotype, Treatment, and their interaction on hnRNP H binding

Deduplicated BAM files were merged across all 12 CLIP samples and deduplicated BAM files were merged across all 12 input (bulk RNA-seq) samples to generate two merged BAM files as the input for peak calling in CLAM as described above. The called peaks were then annotated to the genomic regions as described above. The file containing all the peaks was formatted into a file in GTF format that was used for strand-specific feature counting in individual BAM files from the 12 CLIP samples using featureCounts in the SubRead (Liao et al., 2014). Only peaks with peak intensity > 1.5 and FDR < 0.05 as defined by CLAM were included as 'features' for read counting. Reads were summed for each significant peak to produce a count table containing peaks as rows and samples in columns for differential analysis. To examine the effect of Genotype, Treatment, and their interactive effects on hnRNP H binding, differential analysis was performed using limma (Ritchie et al., 2015) and edgeR (Robinson et al., 2009) based on summed read counts for each peak derived from Subread featureCount. The interactive Genotype and Treatment is expressed as: I = (MUT_MA – MUT_SAL) – (WT_MA – WT_SAL). The positions of the peaks and the corresponding gene targets for effect of Genotype, Treatment, and Genotype x Treatment interaction are found in **Table S3**. The correlation between hnRNP H-associated CLIP peaks in *Hnrnph1* mutants in response to methamphetamine versus wild-types in response to methamphtamine was determined by calculating the Pearson's correlation coefficient.

Differential gene expression and differential exon and intron usage analyses

To triangulate on the CLIP-seq and RNA-seq datasets and associate the downstream effects of hnRNP H binding on gene expression and alternative splicing, we used ASpli (Mancini et al., 2020) to analyze differential gene expression and differential exon/intron usage. Deduplicated BAM files from the 12 total RNA-seq samples were used as inputs for alternative splicing and overall gene expression analysis. To test the general hypothesis that target genes of hnRNPH binding interact with Genotype in response to methamphetamine treatment at the expression or splicing level, the interaction was calculated using the following contrast: I = (MUT_MA – MUT_SAL) – (WT_MA – WT_SAL). The outputs from ASpli can be found in **Table S5** (differential gene expression) and **Table S6** (differential exon and intron usage).

Validation of alternative splicing at the 3'UTR of *Cacna2d2*

For analyzing differential polyadenylation of *Cacna2d2*, the fold-change for each condition relative to saline-treated wild-types was calculated using the $2^{-\Delta\Delta CT}$ method (Livak and Schmittgen, 2001). Three independent replicates were performed for reproducibility. Significance of the RT-qPCR results was determined with a two-way ANCOVA with Genotype and Treatment as between-subject factors with Batch as the co-variate. The

significant main effect of Treatment was followed up with pairwise comparisons separately between wild-types and *Hnrnph1* mutants.

Quantification of CACNA2D2 protein level

The chemiluminescence intensity signal from the immunoblots was quantified using image analysis software, ImageJ. For the Ponceau S stain of total protein stain, the chemiluminescence signal was quantified per lane and used for normalization per lane to determine the protein level of CACNA2D2 in all the samples (Aldridge et al., 2009; Gilda and Gomes, 2013). Three independent replicates were included for reproducibility. Significance of the immunoblot results was determined with a two-way ANCOVA with Genotype and Treatment as between-subject factors with Batch as the co-variate.

Excel Tables

Table S3 (Excel table). RNA-binding targets of hnRNP H. Related to Figures 1, 2, and 3. Differential analysis was performed in limma to identify RNA-binding targets of hnRNP H that showed a main effect of Genotype, Treatment, or interaction. These targets are shown in different tabs in the file.

Table S5 (Excel file). Differential exon and intron usage. Related to Figure 4. A list of differentially spliced genes with differential exon and intron usage as calculated by ASpli showing a Genotype x Treatment interaction [I = (MUT_MA – MUT_SAL) – (WT_MA – WT_SAL)].

Table S6 (Excel file). Differential expressed genes with Genotype x Treatment Interaction. Related to Figure 4. A list of differential expressed genes showing a Genotype x Treatment interaction [I = (MUT_MA – MUT_SAL) – (WT_MA – WT_SAL)].

References

Agarwal, V., Bell, G.W., Nam, J.W., and Bartel, D.P. (2015). Predicting effective microRNA target sites in mammalian mRNAs. Elife *4*, 1–38.

Aldridge, G.M., Podrebarac, D.M., Greenough, W.T., and Weiler, I.J. (2009). The use of total protein stains as loading controls: an alternative to high-abundance single protein controls in semi-quantitative immunoblotting Georgina. J. Neurosci. Methods *172*, 250–254.

Andres, M.A., Cooke, I.M., Bellinger, F.P., Berry, M.J., Zaporteza, M., Rueli, R.H., Barayuga, S.M., and Chang, L. (2015). Methamphetamine acutely inhibits voltage-gated calcium channels but chronically upregulates L-type channels. J Neurochem. *134*, 56–65.

Arhin, G.G.K., Boots, M., Bagga, P.P.S., Milcarek, C., and Wilusz, J. (2002). Downstream sequence elements with different affinities for the hnRNP H/H' protein influence the processing efficiency of mammalian polyadenylation signals. Nucleic Acids Res. *30*, 1842–1850.

Arun, G., Aggarwal, D., and Spector, D.L. (2020). MALAT1 Long Non-Coding RNA: Functional Implications. Non-Coding RNA *6*, 22.

Backlund, M., Stein, F., Rettel, M., Schwarzl, T., Perez-Perri, J.I., Brosig, A., Zhou, Y., Neu-Yilik, G., Hentze, M.W., and Kulozik, A.E. (2020). Plasticity of nuclear and cytoplasmic stress responses of RNA-binding proteins.

Nucleic Acids Res. *48*, 4725–4740.
Bailey, T.L., Boden, M., Buske, F.A., Frith, M., Grant, C.E., Clementi, L., Ren, J., Li, W.W., and Noble, W.S. (2009). MEME Suite: Tools for motif discovery and searching. Nucleic Acids Res. *37*, 202–208.
Bassell, G.J., and Warren, S.T. (2008). Fragile X Syndrome: Loss of Local mRNA Regulation Alters Synaptic Development and Function. Neuron *60*, 201–214.
Batra, R., Manchanda, M., and Swanson, M.S. (2015). Global insights into alternative polyadenylation regulation. RNA Biol. *12*, 597–602.
Baumann, M.H., Ayestas, M.A., Sharpe, L.G., Lewis, D.B., Rice, K.C., and Rothman, R.B. (2002). Persistent antagonism of methamphetamine-induced dopamine release in rats pretreated with GBR12909 decanoate. J. Pharmacol. Exp. Ther. *301*, 1190–1197.
Bernier, F.P., Caluseriu, O., Ng, S., Schwartzentruber, J., Buckingham, K.J., Innes, A.M., Jabs, E.W., Innis, J.W., Schuette, J.L., Gorski, J.L., et al. (2012). Haploinsufficiency of SF3B4, a component of the pre-mRNA spliceosomal complex, causes nager syndrome. Am. J. Hum. Genet. *90*, 925–933.
Bolger, A.M., Lohse, M., and Usadel, B. (2014). Trimmomatic: A flexible trimmer for Illumina sequence data. Bioinformatics *30*, 2114–2120.
Bramham, C.R., and Wells, D.G. (2007). Dendritic mRNA: Transport, translation and function. Nat. Rev. Neurosci. *8*, 776–789.
Bryant, C.D., and Yazdani, N. (2016). RNA binding proteins, neural development and the addictions. Genes Brain Behav. *15*, 169–186.
Bryant, C.D., Parker, C.C., Zhou, L., Olker, C., Chandrasekaran, R.Y., Wager, T.T., Bolivar, V.J., Loudon, A.S., Vitaterna, M.H., Turek, F.W., et al. (2012). Csnk1e is a genetic regulator of sensitivity to psychostimulants and opioids. Neuropsychopharmacology *37*, 1026–1035.
Carboni, G.L., Gao, B., Nishizaki, M., Xu, K., Minna, J.D., Roth, J.A., and Ji, L. (2003). CACNA2D2-mediated apoptosis in NSCLC cells is associated with alterations of the intracellular calcium signaling and disruption of mitochondria membrane integrity. Oncogene *22*, 615–626.
Chen, F., and Keleş, S. (2020). SURF: integrative analysis of a compendium of RNA-seq and CLIP-seq datasets highlights complex governing of alternative transcriptional regulation by RNA-binding proteins. Genome Biol. *21*, 1–23.
Darnell, R.B. (2013). RNA Protein Interaction in Neurons. Annu Rev Neurosci *36*, 243–270.
Darnell, J.C., Driesche, S.J. Van, Zhang, C., Hung, K.Y.S., Mele, A., Fraser, C.E., Stone, E.F., Chen, C., Fak, J.J., Chi, S.W., et al. (2011). FMRP stalls ribosomal translocation on mRNAs linked to synaptic function and autism. Cell *146*, 247–261.
Dassi, E. (2017). Handshakes and fights: The regulatory interplay of RNA-binding proteins. Front. Mol. Biosci. *4*, 1–8.
Dickson, P.E., Miller, M.M., Calton, M.A., Bubier, J.A., Cook, M.N., Goldowitz, D., Chesler, E.J., and Mittleman, G. (2015). Systems genetics of intravenous cocaine self-administration in the BXD recombinant inbred mouse panel. Psychopharmacology (Berl). *233*, 701–714.
Dobin, A., Davis, C.A., Schlesinger, F., Drenkow, J., Zaleski, C., Jha, S., Batut, P., Chaisson, M., and Gingeras,

T.R. (2013). STAR: Ultrafast universal RNA-seq aligner. Bioinformatics *29*, 15–21.
Dolphin, A.C. (2012). Calcium channel auxiliary α2δ and β subunits: Trafficking and one step beyond. Nat. Rev. Neurosci. *13*, 542–555.
Dolphin, A.C. (2013). The α2δ subunits of voltage-gated calcium channels. Biochim. Biophys. Acta - Biomembr. *1828*, 1541–1549.
Dolphin, A.C., and Lee, A. (2020). Presynaptic calcium channels: specialized control of synaptic neurotransmitter release. Nat. Rev. Neurosci. *21*, 213–229.
Ducci, F., and Goldman, D. (2012). The Genetic Basis of Addictive Disorders. Psychiatr. Clin. North Am. *35*, 495–519.
Van Dusen, C.M., Yee, L., McNally, L.M., and McNally, M.T. (2010). A glycine-rich domain of hnRNP H/F promotes nucleocytoplasmic shuttling and nuclear import through an interaction with transportin 1. Mol. Cell. Biol. *30*, 2552–2562.
Fish, E.W., Krouse, M.C., Stringfield, S.J., DiBerto, J.F., Robinson, J.E., and Malanga, C.J. (2013). Changes in Sensitivity of Reward and Motor Behavior to Dopaminergic, Glutamatergic, and Cholinergic Drugs in a Mouse Model of Fragile X Syndrome. PLoS One *8*, 1–14.
Fleckenstein, A.E., and Hanson, G.R. (2003). Impact of psychostimulants on vesicular monoamine transporter function. Eur. J. Pharmacol. *479*, 283–289.
Fleckenstein, A.E., Volz, T.J., and Hanson, G.R. (2009). Psychostimulant-induced alterations in vesicular monoamine transporter-2 function: Neurotoxic and therapeutic implications. Neuropharmacology *56*, 133–138.
Fukuda, T., Naiki, T., Saito, M., and Irie, K. (2009). hnRNP K interacts with RNA binding motif protein 42 and functions in the maintenance of cellular ATP level during stress conditions. Genes to Cells *14*, 113–128.
Fukunaga, T., Iwakiri, J., Ono, Y., and Hamada, M. (2019). Lncrrisearch: A web server for lncRNA-RNA interaction prediction integrated with tissue-specific expression and subcellular localization data. Front. Genet. *10*, 1–6.
Fulks, J.L., Obryhim, B.E., Wenzel, S.K., Fowler, S.C., Vorontsova, E., Pinkston, J.W., Ortiz, A.N., and Johnson, M.A. (2010). Dopamine release and uptake impairments and behavioral alterations observed in mice that model fragile X mental retardation syndrome. ACS Chem. Neurosci. *1*, 679–690.
Galbraith, N. (2015). The methamphetamine problem. BJPsych Bull. *39*, 218–220.
Gelernter, J., Sherva, R., Koesterer, R., Almasy, L., Zhao, H., Kranzler, H.R., and Farrer, L. (2014). Genome-wide association study of cocaine dependence and related traits: FAM53B identified as a risk gene. Mol. Psychiatry *19*, 717–723.
Geuens, T., Bouhy, D., and Timmerman, V. (2016). The hnRNP family: insights into their role in health and disease. Hum. Genet. *135*, 851–867.
Gilda, J.E., and Gomes, A. V. (2013). Stain Free Total Protein Staining is a Superior Loading Control to β-Actin for Western Blots. Anal Biochem. *440*, 1–6.
Goldman, D., Oroszi, G., and Ducci, F. (2005). The genetics of addictions: uncovering the genes. Nat. Rev. Genet. *6*, 521–532.
Guil, S., Long, J.C., and Cáceres, J.F. (2006). hnRNP A1 Relocalization to the Stress Granules Reflects a Role

in the Stress Response. Mol. Cell. Biol. *26*, 5744–5758.
Guramrit, S., Gabriel, P., Gene W., Y., and Melissa J., M. (2015). The Clothes Make the mRNA: Past and Present Trends in mRNP Fashion. Annu. Rev. Biochem. 229–262.
Han, K., Yeo, G., An, P., Burge, C.B., and Grabowski, P.J. (2005). A combinatorial code for splicing silencing: UAGG and GGGG motifs. PLoS Biol. *3*, 0843–0860.
Han, S.P., Tang, Y.H., and Smith, R. (2010). Functional diversity of the hnRNPs: past, present and perspectives. Biochem. J. *430*, 379–392.
Harvey, R.F., Smith, T.S., Mulroney, T., Queiroz, R.M.L., Pizzinga, M., Dezi, V., Villenueva, E., Ramakrishna, M., Lilley, K.S., and Willis, A.E. (2018). Trans-acting translational regulatory RNA binding proteins. Wiley Interdiscip. Rev. RNA *9*, 1–19.
Hedegaard, H., Miniño, A.M., and Warner, M. (2020). Drug Overdose Deaths in the United States, 1999-2018. NCHS Data Brief 1–8.
Heinz, S., Benner, C., Spann, N., Bertolino, E., Lin, Y.C., Laslo, P., Cheng, J.X., Murre, C., Singh, H., and Glass, C.K. (2010). Simple combinations of lineage-determining transcription factors prime cis-regulatory elements required for macrophage and B cell identities. Mol Cell *38*, 576–589.
Hentze, M.W., Castello, A., Schwarzl, T., and Preiss, T. (2018). A brave new world of RNA-binding proteins. Nat. Rev. Mol. Cell Biol. *19*, 327–341.
Honoré, B., Rasmussen, H.H., Vorum, H., Dejgaard, K., Liu, X., Gromov, P., Madsen, P., Gesser, B., Tommerup, N., and Celis, J.E. (1995). Heterogeneous nuclear ribonucleoproteins H, H′, and F are members of a ubiquitously expressed subfamily of related but distinct proteins encoded by genes mapping to different chromosomes. J. Biol. Chem. *270*, 28780–28789.
Hoppa, M.B., Lana, B., Margas, W., Dolphin, A.C., and Ryan, T.A. (2012). α2δ Expression Sets Presynaptic Calcium Channel Abundance and Release Probability. Nature *486*, 122–125.
Huelga, S.C., Vu, A.Q., Arnold, J.D., Liang, T.D., Liu, P.P., Yan, B.Y., Donohue, J.P., Shiue, L., Hoon, S., Brenner, S., et al. (2012). Integrative Genome-wide Analysis Reveals Cooperative Regulation of Alternative Splicing by hnRNP Proteins. Cell Rep. *1*, 167–178.
Hwang, J.Y., Jung, S., Kook, T.L., Rouchka, E.C., Bok, J., and Park, J.W. (2020). rMAPS2: an update of the RNA map analysis and plotting server for alternative splicing regulation. Nucleic Acids Res. *48*, 300–306.
Kamma, H., Portman, D.S.D.S., and Dreyfuss, G. (1995). Cell Type-Specific Expression of hnRNP Proteins. Exp. Cell Res. *221*, 187–196.
Kanehisa, M., Sato, Y., Furumichi, M., Morishima, K., and Tanabe, M. (2019). New approach for understanding genome variations in KEGG. Nucleic Acids Res. *47*, D590–D595.
Karolchik, D., Hinrichs, A.S., Furey, T.S., Roskin, K.M., Sugnet, C.W., Haussler, D., Kent, W.J., and Center (2004). The UCSC Table Browser data retrieval tool. Nucleic Acids Res. *32*, D493–D496.
Katz, Y., Wang, E.T.T., Airoldi, E.M.M., and Burge, C.B.B. (2010). Analysis and design of RNA sequencing experiments for identifying isoform regulation. Nat. Methods *7*, 1009–1015.
Keleta, Y.B., and Martinez, J.L. (2012). Brain Circuits of Methamphetamine Place Reinforcement Learning: The Role of the Hippocampus-VTA Loop. Brain Behav. *2*, 128–141.

Kish, S.J. (2008). Pharmacologic mechanisms of crystal meth. CMAJ *178*, 1679–1682.
Lefave, C. V, Squatrito, M., Vorlova, S., Rocco, G.L., Brennan, C.W., Holland, E.C., Pan, Y., and Cartegni, L. (2011). Splicing factor hnRNPH drives an oncogenic splicing switch in gliomas. EMBO J. *30*, 4084–4097.
Li, M., Shin, J., Risgaard, R.D., Parries, M.J., Wang, J., Chasman, D., Liu, S., Roy, S., Bhattacharyya, A., and Zhao, X. (2020). Identification of FMR1-regulated molecular networks in human neurodevelopment. Genome Res. *30*, 361–374.
Liao, Y., Smyth, G.K., and Shi, W. (2014). FeatureCounts: An efficient general purpose program for assigning sequence reads to genomic features. Bioinformatics *30*, 923–930.
Liao, Y., Wang, J., Jaehnig, E.J., Shi, Z., and Zhang, B. (2019). WebGestalt 2019: gene set analysis toolkit with revamped UIs and APIs. Nucleic Acids Res. *47*, W199–W205.
Lines, M.A., Huang, L., Schwartzentruber, J., Douglas, S.L., Lynch, D.C., Beaulieu, C., Guion-Almeida, M.L., Zechi-Ceide, R.M., Gener, B., Gillessen-Kaesbach, G., et al. (2012). Haploinsufficiency of a spliceosomal GTPase encoded by EFTUD2 causes mandibulofacial dysostosis with microcephaly. Am. J. Hum. Genet. *90*, 369–377.
Livak, K.J., and Schmittgen, T.D. (2001). Analysis of relative gene expression data using real-time quantitative PCR and the 2-ΔΔCT method. Methods *25*, 402–408.
Lominac, K.D., McKenna, C.L., Schwartz, L.M., Ruiz, P.N., Wroten, M.G., Miller, B.W., Holloway, J.J., Travis, K.O., Rajasekar, G., Maliniak, D., et al. (2014). Mesocorticolimbic monoamine correlates of methamphetamine sensitization and motivation. Front. Syst. Neurosci. *8*, 1–19.
Mancini, E., Rabinovich, A., Iserte, J., and Yanovsky, M. (2020). ASpli: Analysis of alternative splicing using RNA-Seq. R Packag. Version 1.14.0.
Markmiller, S., Soltanieh, S., Server, K.L., Mak, R., Jin, W.J., Fang, M.Y., Luo, E.-C., Krach, F., Yang, D., Sen, A., et al. (2018). Context-Dependent and Disease-Specific Diversity in Protein Interactions within Stress Granules. Cell *172*, 590–604.
Mayr, C. (2017). Regulation by 3 -Untranslated Regions. Annu. Rev. *51*, 171–194.
Merico, D., Isserlin, R., Stueker, O., Emili, A., and Bader, G.D. (2010). Enrichment map: A network-based method for gene-set enrichment visualization and interpretation. PLoS One *5*, e13984.
Muddashetty, R.S., Nalavadi, V.C., Gross, C., Yao, X., Xing, L., Laur, O., Warren, S.T., and Bassell, G.J. (2011). Reversible Inhibition of PSD-95 mRNA Translation by miR-125a, FMRP Phosphorylation, and mGluR Signaling. Mol. Cell *42*, 673–688.
Van Nostrand, E.L., Pratt, G.A., Shishkin, A.A., Gelboin-, C., Fang, M.Y., Sundararaman, B., Blue, S.M., Thai, B., Surka, C., Elkins, K., et al. (2016). Robust transcriptome-wide discovery of RNA binding protein binding sites with enhanced CLIP (eCLIP). Nat. Methods *13*, 508–514.
Pilch, J., Koppolu, A.A., Walczak, A., Murcia Pienkowski, V.A., Biernacka, A., Skiba, P., Machnik-Broncel, J., Gasperowicz, P., Kosińska, J., Rydzanicz, M., et al. (2018). Evidence for HNRNPH1 being another gene for Bain type syndromic mental retardation. Clin. Genet. *94*, 381–385.
Qian, H., Kang, X., Hu, J., Zhang, D., Liang, Z., Meng, F., Zhang, X., Xue, Y., Maimon, R., Dowdy, S.F., et al. (2020). Reversing a model of Parkinson ' s disease with in situ converted nigral neurons. Nature *582*.

Quinlan, A.R., and Hall, I.M. (2010). BEDTools: A flexible suite of utilities for comparing genomic features. Bioinformatics *26*, 841–842.

Raudvere, U., Kolberg, L., Kuzmin, I., Arak, T., Adler, P., Peterson, H., and Vilo, J. (2019). G:Profiler: A web server for functional enrichment analysis and conversions of gene lists (2019 update). Nucleic Acids Res. *47*, W191–W198.

Reed, C., Baba, H., Zhu, Z., Erk, J., Mootz, J.R., Varra, N.M., Williams, R.W., and Phillips, T.J. (2018). A spontaneous mutation in Taar1 impacts methamphetamine-related traits exclusively in DBA/2 mice from a single vendor. Front. Pharmacol. *8*, 1–18.

Reichert, S.C., Li, R., A. Turner, S., van Jaarsveld, R.H., Massink, M.P.G., van den Boogaard, M.J.H., del Toro, M., Rodríguez-Palmero, A., Fourcade, S., Schlüter, A., et al. (2020). HNRNPH1-related syndromic intellectual disability: Seven additional cases suggestive of a distinct syndromic neurodevelopmental syndrome. Clin. Genet. *98*, 91–98.

Reimand, J., Isserlin, R., Voisin, V., Kucera, M., Tannus-Lopes, C., Rostamianfar, A., Wadi, L., Meyer, M., Wong, J., Xu, C., et al. (2019). Pathway enrichment analysis and visualization of omics data using g:Profiler, GSEA, Cytoscape and EnrichmentMap. Nat. Protoc. *14*, 482–517.

Rieger, M.A., King, D.M., Crosby, H., Liu, Y., Cohen, B.A., and Dougherty, J.D. (2020). CLIP and Massively Parallel Functional Analysis of CELF6 Reveal a Role in Destabilizing Synaptic Gene mRNAs through Interaction with 3′ UTR Elements. Cell Rep. *33*, 108531.

Ritchie, M.E., Phipson, B., Wu, D., Hu, Y., Law, C.W., Shi, W., and Smyth, G.K. (2015). Limma powers differential expression analyses for RNA-sequencing and microarray studies. Nucleic Acids Res. *43*, e47.

Rizzuto, R., De Stefani, D., Raffaello, A., and Mammucari, C. (2012). Mitochondria as sensors and regulators of calcium signalling. Nat. Rev. Mol. Cell Biol. *13*, 566–578.

Robinson, M.D., McCarthy, D.J., and Smyth, G.K. (2009). edgeR: A Bioconductor package for differential expression analysis of digital gene expression data. Bioinformatics *26*, 139–140.

Ruan, Q.T., Yazdani, N., Beierle, J.A., Hixson, K.M., Hokenson, K.E., Apicco, D.J., Luttik, K.P., Zheng, K., Maziuk, B.F., Ash, P.E.A., et al. (2018). Changes in neuronal immunofluorescence in the C- versus N-terminal domains of hnRNP H following D1 dopamine receptor activation. Neurosci. Lett. *684*, 109–114.

Ruan, Q.T., Yazdani, N., Blum, B.C., Beierle, J.A., Lin, W., Coelho, M.A., Fultz, E.K., Healy, A.F., Shahin, J.R., Kandola, A.K., et al. (2020a). A mutation in hnRNPH1 that decreases methamphetamine-induced reinforcement, reward, and dopamine release and increases synaptosomal hnRNP H and mitochondrial proteins. J. Neurosci. *40*, 107–130.

Ruan, Q.T., Yazdani, N., Reed, E.R., Beierle, J.A., Peterson, L.P., Luttik, K.P., Szumlinski, K.K., Johnson, W.E., Ash, P.E.A., Wolozin, B., et al. (2020b). 5′ UTR variants in the quantitative trait gene Hnrnph1 support reduced 5′ UTR usage and hnRNP H protein as a molecular mechanism underlying reduced methamphetamine sensitivity. FASEB J. *34*, 9223–9244.

Russo, A., Siciliano, G., Catillo, M., Giangrande, C., Amoresano, A., Pucci, P., Pietropaolo, C., and Russo, G. (2010). hnRNP H1 and intronic G runs in the splicing control of the human rpL3 gene. Biochim. Biophys. Acta - Gene Regul. Mech. *1799*, 419–428.

Scherer, M., Levin, M., Butter, F., and Scheibe, M. (2020). Quantitative proteomics to identify nuclear rna-binding proteins of malat1. Int. J. Mol. Sci. *21*, 1–12.
Shi, X., Walter, N.A.R., Harkness, J.H., Neve, K.A., Williams, R.W., Lu, L., Belknap, J.K., Eshleman, A.J., Phillips, T.J., and Janowsky, A. (2016). Genetic polymorphisms affect mouse and human trace amine-associated receptor 1 function. PLoS One *11*, 1–14.
Siciliano, C.A., Calipari, E.S., Ferris, M.J., and Jones, S.R. (2014). Biphasic mechanisms of amphetamine action at the dopamine terminal. J. Neurosci. *34*, 5575–5582.
Smith, L.N., Jedynak, J.P., Fontenot, M.R., Hale, C.F., Dietz, K.C., Taniguchi, M., Thomas, F.S., Zirlin, B.C., Birnbaum, S.G., Huber, M., et al. (2014). Fragile X mental retardation protein regulates synaptic and behavioral plasticity to repeated cocaine administration. Neuron *82*, 645–658.
Smith, T., Heger, A., and Sudbery, I. (2017). UMI-tools: Modelling sequencing errors in Unique Molecular Identifiers to improve quantification accuracy. Genome Res. *27*.
Team, R.C. (2013). R: A language and environment for statistical computing. R Found. Stat. Comput. Vienna, Austria.
Thorvaldsdóttir, H., Robinson, J.T., and Mesirov, J.P. (2013). Integrative Genomics Viewer (IGV): High-performance genomics data visualization and exploration. Brief. Bioinform. *14*, 178–192.
Uren, P.J., Bahrami-Samani, E., de Araujo, P.R., Vogel, C., Qiao, M., Burns, S.C., Smith, A.D., and Penalva, L.O.F. (2016). High-throughput analyses of hnRNP H1 dissects its multi-functional aspect. RNA Biol. 1–12.
Verkerk, A.J.M.H., Pieretti, M., Sutcliffe, J.S., Fu, Y.H., Kuhl, D.P.A., Pizzuti, A., Reiner, O., Richards, S., Victoria, M.F., Zhang, F., et al. (1991). Identification of a gene (FMR-1) containing a CGG repeat coincident with a breakpoint cluster region exhibiting length variation in fragile X syndrome. Cell *65*, 905–914.
Wall, M.L., Bera, A., Wong, F.K., and Lewis, S.M. (2020). Cellular stress orchestrates the localization of hnRNP H to stress granules. Exp. Cell Res. *394*, 112111.
Wang, H., Wu, L.J., Kim, S.S., Lee, F.J.S., Gong, B., Toyoda, H., Ren, M., Shang, Y.Z., Xu, H., Liu, F., et al. (2008). FMRP Acts as a Key Messenger for Dopamine Modulation in the Forebrain. Neuron *59*, 634–647.
Wang, H., Kim, S.S., and Zhuo, M. (2010). Roles of fragile X mental retardation protein in dopaminergic stimulation-induced synapse-associated protein synthesis and subsequent α-amino-3-hydroxyl-5-methyl-4-isoxazole-4-propionate (AMPA) receptor internalization. J. Biol. Chem. *285*, 21888–21901.
Wise, R.A. (2004). Dopamine, learning and motivation. Nat. Rev. Neurosci. *5*, 483–494.
Xu, J., Lu, Z., Xu, M., Pan, L., Deng, Y.Y., Xie, X., Liu, H., Ding, S., Hurd, Y.L., Gavril, X., et al. (2014). A Heroin Addiction Severity-Associated Intronic Single Nucleotide Polymorphism Modulates Alternative Pre-mRNA Splicing of the Opioid Receptor Gene OPRM1 via hnRNPH Interactions. J. Neurosci. *34*, 11048–11066.
Yazdani, N., Parker, C.C., Shen, Y., Reed, E.R., Guido, M.A., Kole, L.A., Kirkpatrick, S.L., Lim, J.E., Sokoloff, G., Cheng, R., et al. (2015). Hnrnph1 Is A Quantitative Trait Gene for Methamphetamine Sensitivity. PLoS Genet. *11*, e1005713.
Yorgason, J.T., Hedges, D.M., Obray, J.D., Jang, E.Y., Bills, K.B., Woodbury, M., Williams, B., Parsons, M.J., Andres, M.A., and Steffensen, S.C. (2020). Methamphetamine increases dopamine release in the nucleus accumbens through calcium-dependent processes. Psychopharmacology (Berl). *237*, 1317–1330.

Zhang, Z., and Xing, Y. (2017). CLIP-seq analysis of multi-mapped reads discovers novel functional RNA regulatory sites in the human transcriptome. Nucleic Acids Res. *45*, 9260–9271.

Zhang, X., Hamblin, M.H., and Yin, K.J. (2017). The long noncoding RNA Malat1: Its physiological and pathophysiological functions. RNA Biol. *14*, 1705–1714.

Zhou, Z., Karlsson, C., Liang, T., Xiong, W., Kimura, M., Tapocik, J.D., Yuan, Q., Barbier, E., Feng, A., Flanigan, M., et al. (2013). Loss of metabotropic glutamate receptor 2 escalates alcohol consumption. Proc. Natl. Acad. Sci. U. S. A. *110*, 16963–16968.

Figure 1

A

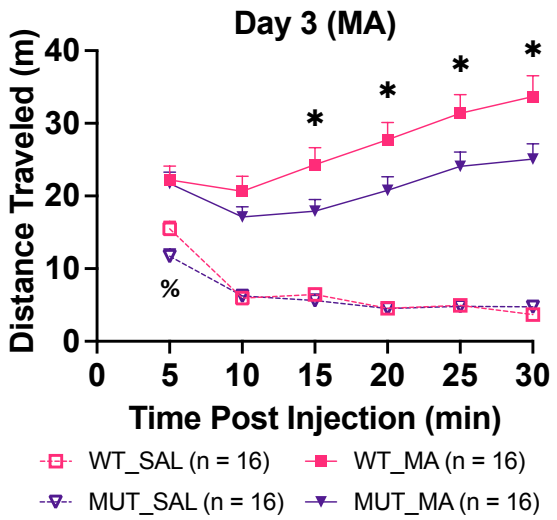

B

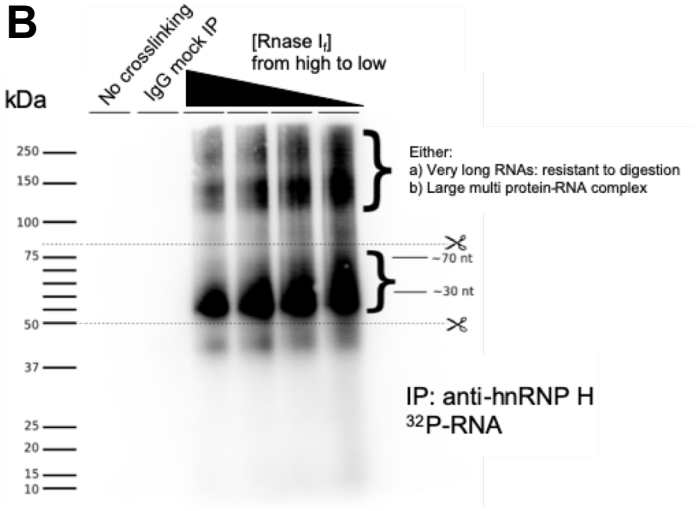

C

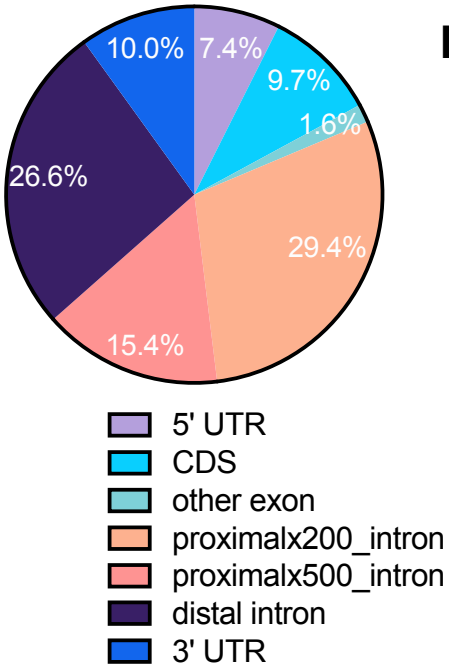

D

Rank	Motif	p value	% of targets
1		1E-129	14.21%
2		1E-108	5.78%
3		1E-102	20.44%
4		1E-101	46.28%
5		1E-71	3.00%

E **hnRNP H-associated targets with G-rich motif in WT_SAL**

Top 10 Pathways by Enrichment Ratio (FDR > 0.05)

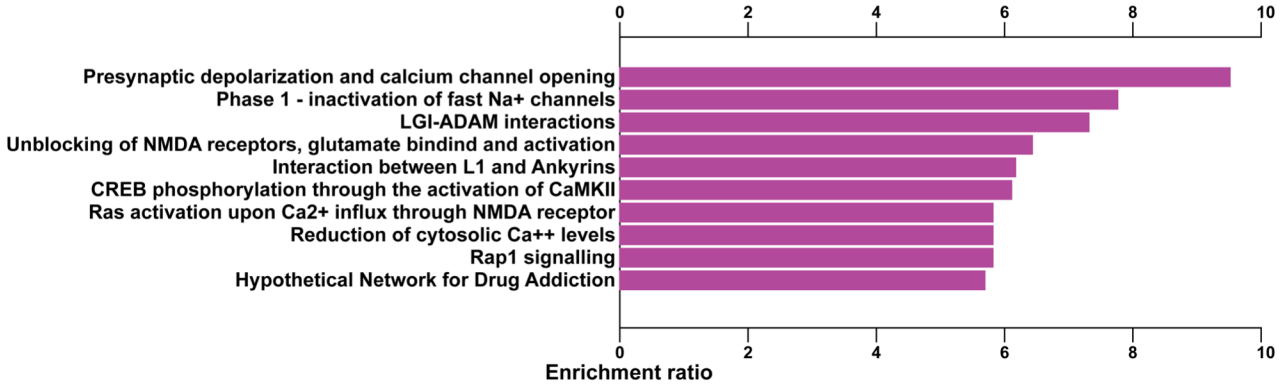

Figure 2

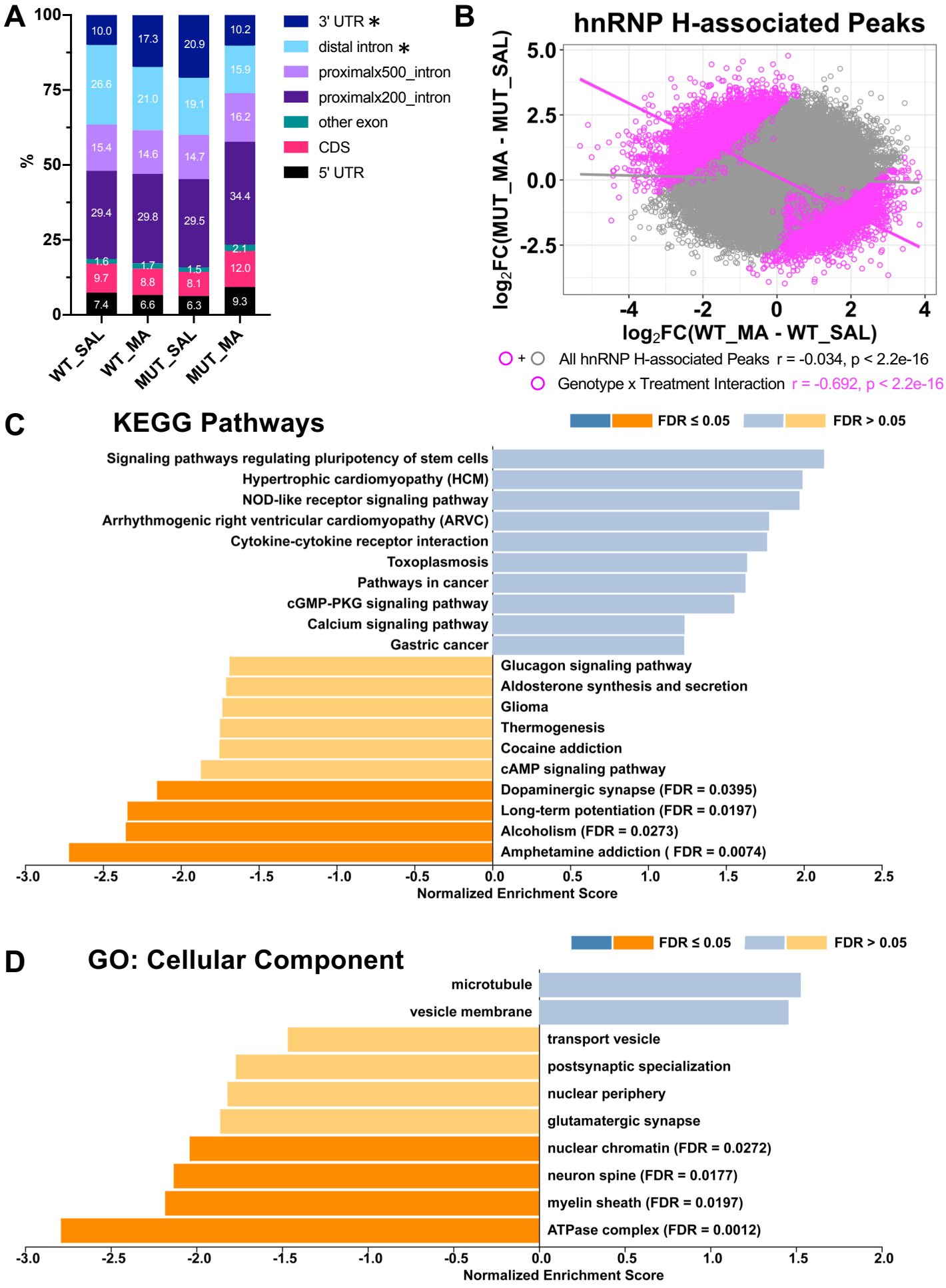
A
100
75
50
25
0
%
10.0
26.6
15.4
29.4
1.6
9.7
7.4
17.3
21.0
14.6
29.8
1.7
8.8
6.6
20.9
19.1
14.7
29.5
1.5
8.1
6.3
10.2
15.9
16.2
34.4
2.1
12.0
9.3
WT_SAL
WT_MA
MUT_SAL
MUT_MA
3' UTR *
distal intron *
proximalx500_intron
proximalx200_intron
other exon
CDS
5' UTR
B
hnRNP H-associated Peaks
log2FC(MUT_MA - MUT_SAL)
5.0
2.5
0.0
-2.5
-4
-2
0
2
4
log2FC(WT_MA - WT_SAL)
+
All hnRNP H-associated Peaks r = -0.034, p < 2.2e-16
Genotype x Treatment Interaction r = -0.692, p < 2.2e-16
C
KEGG Pathways
FDR ≤ 0.05
FDR > 0.05
Signaling pathways regulating pluripotency of stem cells
Hypertrophic cardiomyopathy (HCM)
NOD-like receptor signaling pathway
Arrhythmogenic right ventricular cardiomyopathy (ARVC)
Cytokine-cytokine receptor interaction
Toxoplasmosis
Pathways in cancer
cGMP-PKG signaling pathway
Calcium signaling pathway
Gastric cancer
Glucagon signaling pathway
Aldosterone synthesis and secretion
Glioma
Thermogenesis
Cocaine addiction
cAMP signaling pathway
Dopaminergic synapse (FDR = 0.0395)
Long-term potentiation (FDR = 0.0197)
Alcoholism (FDR = 0.0273)
Amphetamine addiction (FDR = 0.0074)
-3.0
-2.5
-2.0
-1.5
-1.0
-0.5
0.0
0.5
1.0
1.5
2.0
2.5
Normalized Enrichment Score
D
GO: Cellular Component
FDR ≤ 0.05
FDR > 0.05
microtubule
vesicle membrane
transport vesicle
postsynaptic specialization
nuclear periphery
glutamatergic synapse
nuclear chromatin (FDR = 0.0272)
neuron spine (FDR = 0.0177)
myelin sheath (FDR = 0.0197)
ATPase complex (FDR = 0.0012)
-3.0
-2.5
-2.0
-1.5
-1.0
-0.5
0.0
0.5
1.0
1.5
2.0
Normalized Enrichment Score

Figure 3

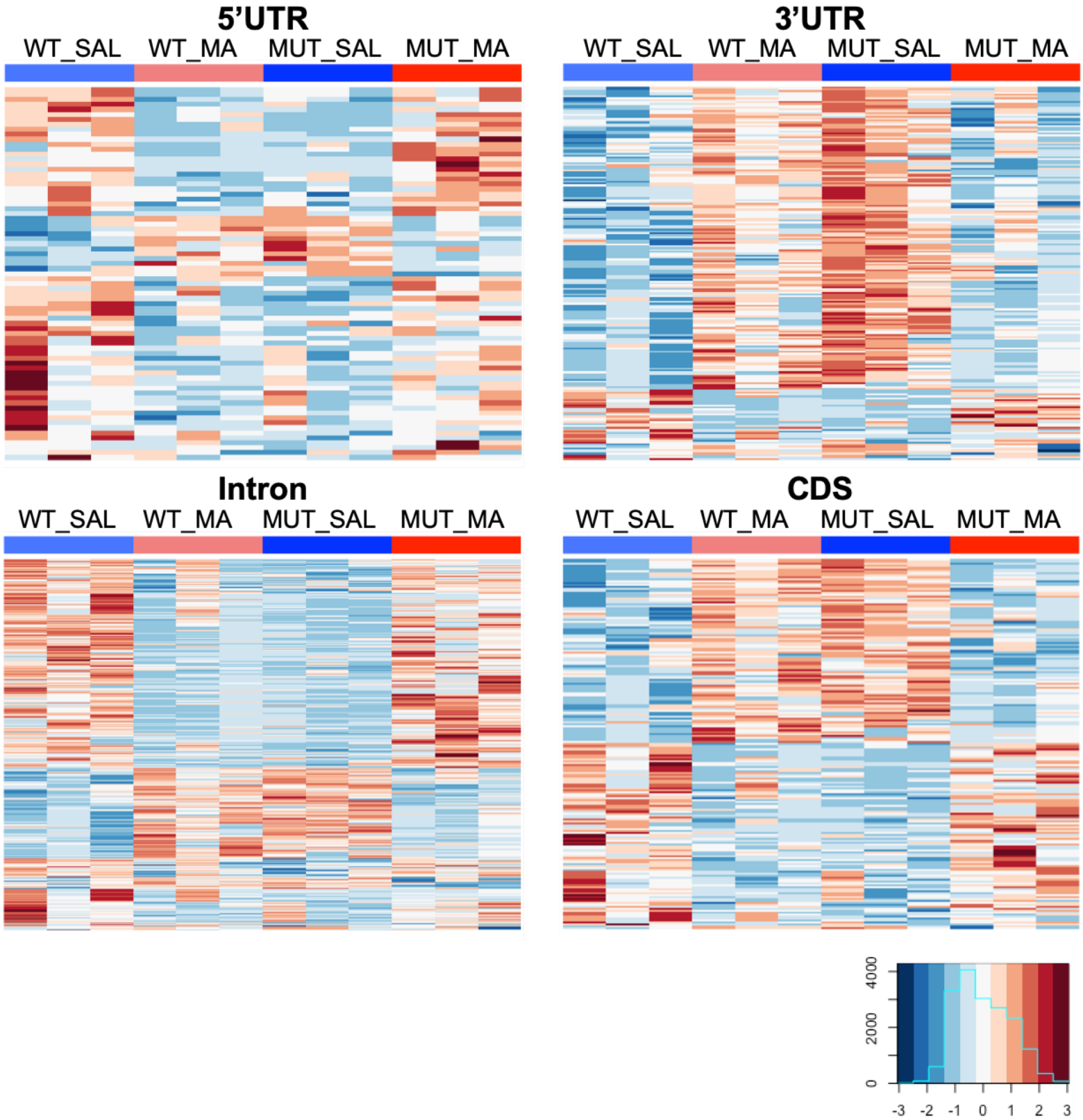
5'UTR
WT_SAL
WT_MA
MUT_SAL
MUT_MA
3'UTR
WT_SAL
WT_MA
MUT_SAL
MUT_MA
Intron
WT_SAL
WT_MA
MUT_SAL
MUT_MA
CDS
WT_SAL
WT_MA
MUT_SAL
MUT_MA
0
2000
4000
-3
-2
-1
0
1
2
3

Table 1. KEGG Enrichment analysis of dynamic hnRNP H 3'UTR targets. The table shows those 3'UTR RNA targets responding to the interaction of Genotype and Treatment. The interaction is expressed as $(MUT_{MA} – MUT_{SAL}) – (WT_{MA} – WT_{SAL})$ with $p < 0.01$.

Pathway	Adjusted p	RNA targets
Long-term potentiation	1.36E-06	*Braf, Prkcb, Grm5, Ppp3r1, Hras, Gria2, Gnaq, Grin2a, Calm2*
Glutamatergic synapse	5.69E-06	*Gnas, Prkcb, Slc38a1, Grm5, Ppp3r1, Gria2, Gnaq, Grin2a, Slc1a3, Slc1a2*
Long-term depression	7.15E-05	*Gnas, Braf, Prkcb, Hras, Gria2, Gnaq, Ppp2r1b*
Salivary secretion	2.87E-04	*Gnas, Prkcb, Atp1b1, Atp1b2, Gnaq, Calm2, Vamp2*
Dopaminergic synapse	9.51E-04	*Gnas, Prkcb, Ppp2r5b, Gria2, Gnaq, Ppp2r1b, Grin2a, Calm2*
Aldosterone synthesis and secretion	9.51E-04	*Gnas, Prkcb, Pde2a, Atp1b1, Atp1b2, Gnaq, Calm2*
Amphetamine addiction	9.51E-04	*Gnas, Prkcb, Ppp3r1, Gria2, Grin2a, Calm2*
Gastric acid secretion	1.24E-03	*Gnas, Prkcb, Atp1b1, Atp1b2, Gnaq, Calm2*
Synaptic vesicle cycle	1.31E-03	*Atp6v1b2, Slc6a1, Slc1a3, Atp6v0c, Vamp2, Slc1a2*
Cocaine addiction	1.31E-03	*Gnas, Rgs9, Gria2, Cdk5r1,Grin2a*

Table 2. KEGG Enrichment analysis of dynamic hnRNP H intronic targets. The table shows those intronic RNA targets responding to the interaction of Genotype and Treatment. The interaction is expressed as $(MUT_{MA} – MUT_{SAL}) – (WT_{MA} – WT_{SAL})$ with $p < 0.01$.

Pathway	Adjusted p	RNA targets
Oxytocin signaling pathway	1.31E-11	*Prkag2, Itpr1, Prkcb, Rock1, Cacnb2, Plcb1, Adcy5, Cacng2, Ryr2, Ppp1cb, Ppp3ca, Kcnj4, Camk1d, Ppp3r1, Cacna2d4, Cacna2d3, Cacna1d, Ppp1r12c, Camk4, Elk1, Camk2a, Map2k2, Cacna1c, Cacnb4, Gnas, Cacng8, Prkag1, Ppp3cb, Cacnb1, Hras, Rock2, Adcy6, Calm2, Plcb4*
Long-term potentiation	6.66E-09	*Itpr1, Prkcb, Gria1, Grin2b, Plcb1, Grin2a, Ppp1cb, Ppp3ca, Ppp3r1, Camk4, Camk2a, Map2k2, Cacna1c, Grin2d, Gria2, Ppp3cb, Hras, Calm2, Plcb4*
Glutamatergic synapse	7.93E-09	*Itpr1, Prkcb, Gria1, Grin2b, Plcb1, Adcy5, Grm4, Grin2a, Slc1a3, Ppp3ca, Gng7, Dlgap1, Ppp3r1, Grik5, Cacna1d, Cacna1c, Grin2d, Gria2, Gnas, Ppp3cb, Adcy6, Cacna1a, Slc38a3, Plcb4, Slc1a1*
Dopaminergic synapse	1.70E-08	*Itpr1, Prkcb, Gria1, Ppp1r1b, Grin2b, Plcb1, Mapk10, Adcy5, Grin2a, Ppp1cb, Ppp3ca, Gng7, Ppp2cb, Kif5c, Cacna1d, Mapk14, Camk2a, Cacna1c, Gria2, Gnas, Scn1a, Ppp3cb, Cacna1a, Calm2, Ppp2r2d, Plcb4, Ppp2r1b*
Adrenergic signaling in cardiomyocytes	3.34E-08	*Atp2b2, Cacnb2, Plcb1, Adcy5, Cacng2, Scn7a, Slc8a1, Ryr2, Ppp1cb, Cacna2d4, Cacna2d3, Ppp2cb, Cacna1d, Mapk14, Scn4b, Camk2a, Cacna1c, Atp1a2, Cacnb4, Gnas, Cacng8, Cacnb1, Adcy6, Calm2, Ppp2r2d, Plcb4, Atp1b2, Ppp2r1b*
Amphetamine addiction	5.46E-08	*Prkcb, Gria1, Ppp1r1b, Grin2b, Adcy5, Grin2a, Ppp1cb, Ppp3ca, Ppp3r1, Cacna1d, Camk4, Camk2a, Cacna1c, Grin2d, Gria2, Gnas, Ppp3cb, Calm2*
Circadian entrainment	1.88E-07	*Itpr1, Prkcb, Gria1, Grin2b, Plcb1, Nos1ap, Adcy5, Ryr2, Grin2a, Gng7, Cacna1h, Cacna1d, Camk2a, Cacna1c, Grin2d, Gria2, Gnas, Per1, Adcy6, Calm2, Plcb4*
cGMP-PKG signaling pathway	6.19E-07	*Itpr1, Atp2b2, Rock1, Prkce, Pde2a, Plcb1, Slc8a3, Adcy5, Mef2d, Slc8a1, Ppp1cb, Ppp3ca, Ppp3r1, Slc8a2, Cacna1d, Insr, Gna13, Map2k2, Cacna1c, Atp1a2, Mef2b, Ednra, Ppp3cb, Rock2, Adcy6, Calm2, Plcb4, Atp1b2*
Arrhythmogenic right ventricular cardiomyopathy (ARVC)	7.64E-07	*Cacnb2, Sgcd, Cacng2, Slc8a1, Ryr2, Cacna2d4, Ctnna2, Cacna2d3, Cacna1d, Dag1, Cacna1c, Cacnb4, Itgb8, Cacng8, Cacnb1, Gja1, Itga9*
Calcium signaling pathway	1.29E-06	*Itpr1, Prkcb, Atp2b2, Plcb1, Pde1a, Slc8a3, Htr2c, Slc8a1, Ryr2, Grin2a, Ppp3ca, Ppp3r1, Slc8a2, Cacna1h, Cacna1d, Camk4, Camk2a, Cacna1c, Chrna7, Grin2d, Ednra, Gnas, Ppp3cb, Cacna1a, Calm2, Itpka, Plcb4, Pde1b, Ptk2b*

Figure 4

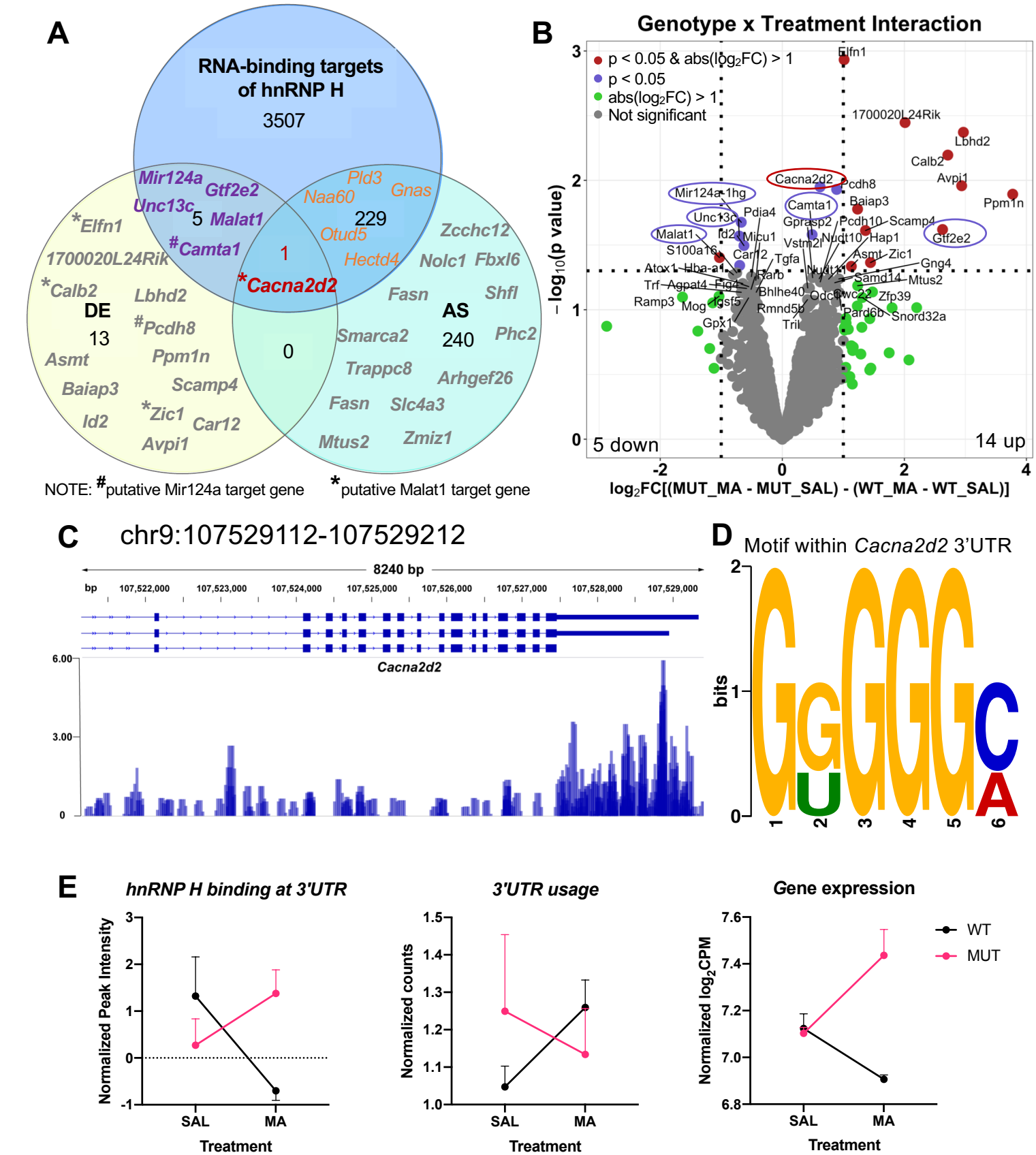

A
RNA-binding targets of hnRNP H
3507
Mir124a
Gtf2e2
Unc13c
5
Malat1
#Camta1
*Elfn1
1700020L24Rik
*Calb2
Lbhd2
DE
13
#Pcdh8
Asmt
Ppm1n
Baiap3
Scamp4
*Zic1
Id2
Car12
Avpi1
Pld3
Naa60
Gnas
229
Otud5
1
Hectd4
*Cacna2d2
Zcchc12
Nolc1
Fbxl6
Fasn
Shfl
AS
240
Phc2
Smarca2
0
Trappc8
Arhgef26
Fasn
Slc4a3
Mtus2
Zmiz1
NOTE: #putative Mir124a target gene
*putative Malat1 target gene
B
Genotype x Treatment Interaction
p < 0.05 & abs(log2FC) > 1
p < 0.05
abs(log2FC) > 1
Not significant
Elfn1
1700020L24Rik
Lbhd2
Calb2
Avpi1
Ppm1n
Cacna2d2
Pcdh8
Mir124a-1hg
Camta1
Baiap3
Unc13c
Pdia4
Gprasp2
Pcdh10
Scamp4
Malat1
Id2
Micu1
Vstm2l
Nudt10
Hap1
Gtf2e2
S100a16
Car12
Tgfa
Asmt
Zic1
Gng4
Atox1
Hba-a1
Rarb
Nudt11
Samd14
Mtus2
Trf
Agpat4
Fig4
Bhlhe40
Odc1
Cwc22
Zfp39
Ramp3
Mog
Igsf5
Rmnd5b
Pard6b
Snord32a
Gpx1
Tril
5 down
14 up
−log10(p value)
log2FC[(MUT_MA - MUT_SAL) - (WT_MA - WT_SAL)]
C
chr9:107529112-107529212
8240 bp
bp
107,522,000
107,523,000
107,524,000
107,525,000
107,526,000
107,527,000
107,528,000
107,529,000
Cacna2d2
6.00
3.00
0
D
Motif within Cacna2d2 3'UTR
bits
E
hnRNP H binding at 3'UTR
Normalized Peak Intensity
SAL
MA
Treatment
3'UTR usage
Normalized counts
Gene expression
Normalized log2CPM
WT
MUT

Figure 5

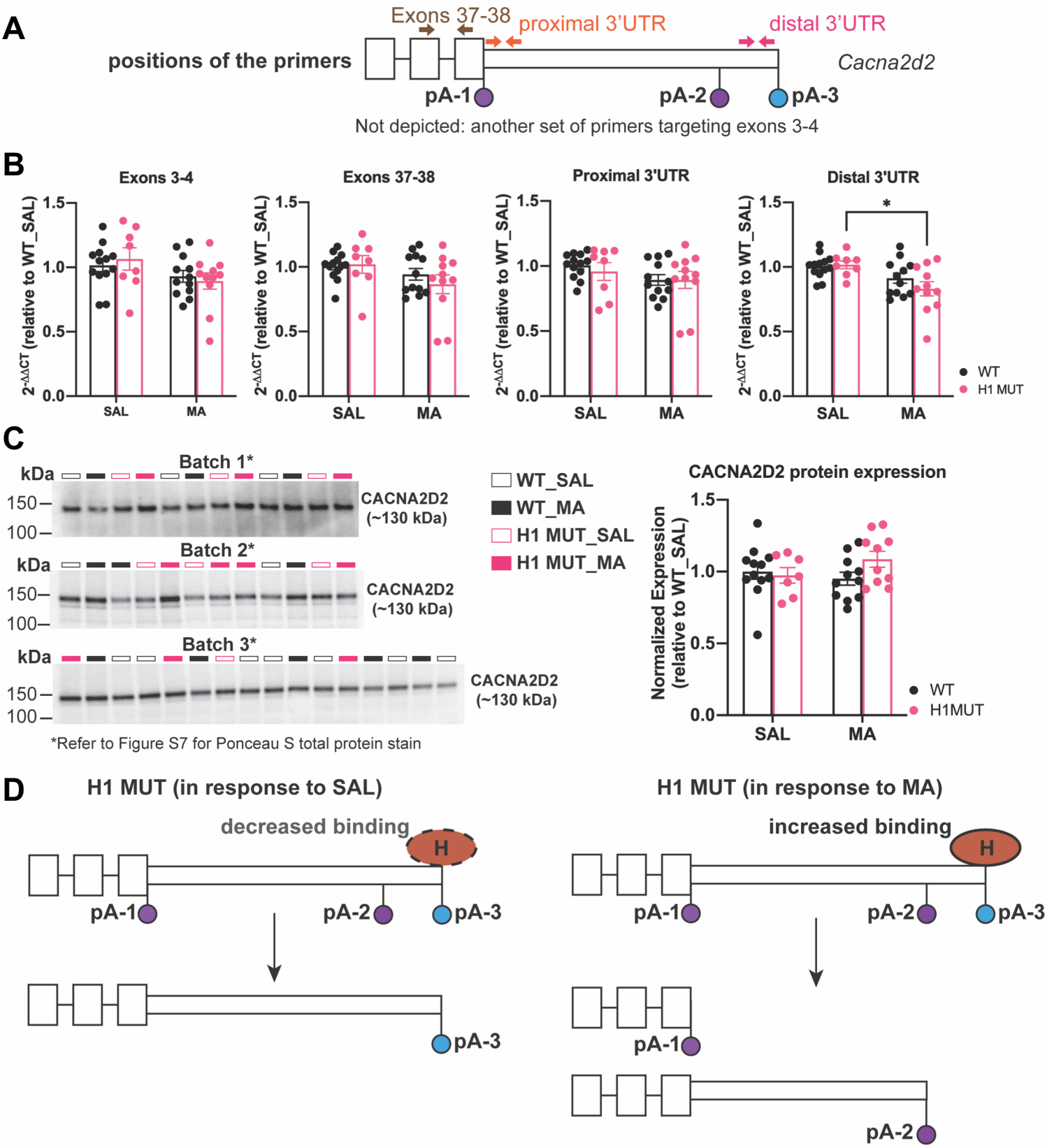
A
positions of the primers
Exons 37-38
proximal 3'UTR
distal 3'UTR
Cacna2d2
pA-1
pA-2
pA-3
Not depicted: another set of primers targeting exons 3-4
B
Exons 3-4
Exons 37-38
Proximal 3'UTR
Distal 3'UTR
2^-ΔΔCT (relative to WT_SAL)
SAL
MA
WT
H1 MUT
C
Batch 1*
Batch 2*
Batch 3*
kDa
150
100
CACNA2D2 (~130 kDa)
WT_SAL
WT_MA
H1 MUT_SAL
H1 MUT_MA
CACNA2D2 protein expression
Normalized Expression (relative to WT_SAL)
H1MUT
*Refer to Figure S7 for Ponceau S total protein stain
D
H1 MUT (in response to SAL)
decreased binding
H1 MUT (in response to MA)
increased binding
H